Biomaterials Translational

Electrical stimulation with polypyrrole-coated polycaprolactone/silk fibroin scaffold promotes sacral nerve regeneration by modulating macrophage polarisation

Haofeng Cheng[1,2,3,4,#], Jun Bai[2,3,4,#], Xingyu Zhou[1,2,3,4,#], Nantian Chen[1,2,3,4], Qingyu Jiang[2,3], Zhiqi Ren[2,3], Xiangling Li[3], Tianqi Su[2,3], Lijing Liang[3,5,6], Wenli Jiang[6], Yu Wang[3,4,], Jiang Peng[3,4,*], Aijia Shang[1,2,*]*

Key Words:
electrical stimulation; JAK-STAT signalling pathway; macrophage polarisation; peripheral nerve regeneration; polypyrrole; sacral nerve injury

From the Contents

ABSTRACT

Peripheral nerve injury poses a great threat to neurosurgery and limits the regenerative potential of sacral nerves in the neurogenic bladder. It remains unknown whether electrical stimulation can facilitate sacral nerve regeneration in addition to modulate bladder function. The objective of this study was to utilise electrical stimulation in sacra nerve crush injury with newly constructed electroconductive scaffold and explore the role of macrophages in electrical stimulation with crushed nerves. As a result, we generated a polypyrrole-coated polycaprolactone/silk fibroin scaffold through which we applied electrical stimulation. The electrical stimulation boosted nerve regeneration and polarised the macrophages towards the M2 phenotype. An in vitro test using bone marrow derived macrophages revealed that the pro-regenerative polarisation of M2 were significantly enhanced by electrical stimulation. Bioinformatics analysis showed that the expression of signal transducer and activator of transcriptions (STATs) was differentially regulated in a way that promoted M2-related genes expression. Our work indicated the feasibility of electricals stimulation used for sacral nerve regeneration and provided a firm demonstration of a pivotal role which macrophages played in electrical stimulation.

http://doi.org/10.12336/biomatertransl.2024.02.006

How to cite this article:
Cheng, H.; Bai, J.; Zhou, X.; Chen, N.; Jiang, Q.; Ren, Z.; Li, X.; Su, T.; Liang, L.; Jiang, W.; Wang, Y.; Peng J.; Shang, A. Electrical stimulation with polypyrrole-coated polycaprolactone/silk fibroin scaffold promotes sacral nerve regeneration by modulating macrophage polarisation. *Biomater Transl.* **2024**, *5*(2), 157-174.

Introduction

The treatment of peripheral nerve injury is a major clinical challenge due to the limited nerve regenerative potential and nerve graft sources. There have been great advances in tissue engineering and implantable artificial biomaterials for treatment of branchial plexus or sciatic nerve injuries. Treatment of sacral nerve injury that is due to spinal bifida, tethered cord syndrome and sacral fracture, which leads to urinary dysfunctions, is very challenging.[1] Compared with other nerve injuries that usually cause motor dysfunctions, the sacral nerve is a mixed nerve comprising motor, sensory and autonomic nerves (parasympathetic nerves) that mainly innervate the bladder and bowel. Damage to autonomic nerve fibres in the sacral nerve can lead to detrusor underactivity and cause neurogenic bladder.[2-4]

Injury to peripheral nerves with regenerative potential can result in incomplete functional recovery.[5] The prevailing theory focuses on microenvironment, which is initially pro-inflammatory but evolves into the pro-regeneration state.[6] The window phase inhibits the nerve fibre from reaching the far-end,

resulting in neural degeneration of the distal stump. The microenvironment encloses the nerve fibres that coordinate axon elongation and myelination,[7, 8] where immune cells such as macrophages, neutrophils and lymph cells of diverse phenotypes are highly involved. Macrophages act as a switch between pro-inflammatory and pro-regeneration states.[9-13] Inflammatory monocytes are recruited from the blood by multiple chemokines and differentiate into macrophages, which would intermingle with resident macrophages to be activated and clustered into certain groups with symbolic marker and function. The complicated macrophage polarisation was conventionally summarised as M1/M2 phenotypes. Classically activated macrophages (M1) express *Tnfa, Il1b, Il6,* as well as *Il12* and help clear debris and eliminate apoptotic cells, that is to say, aggravate inflammation. Alternatively activated macrophages, which are marked with *Retnla, Mrc1, Ym1* and *Arg1* facilitate the extension of axons and secretion of growth factors.[14] Manipulation of macrophage polarisation can impact the regeneration process, as the previous studies prevailed.

Electrical stimulation (ES) has promising therapeutic effects on peripheral nerve injury.[8, 15] Clinical trials involving median, digital, ulnar, brachial plexus and facial nerves have reported on the significance of ES in promoting peripheral nerve injury regeneration,[16] however, the involved mechanisms have yet to be reported. It has been postulated that ES helps restore the balance of neuronal potentials under certain electrical fields. Zhao et al.[17] found that direct current ES promoted Schwann cell proliferation, migration as well as remyelination via the activation of mitogen-activated protein kinase (MAPK) signalling pathway. In our previous study, ES enhanced Wallerian degeneration.[18] However, these studies did not report on the significance of macrophages, which regulate microenvironmental regeneration Macrophage polarisation can be manipulated via physical or chemical stimulation, including ES. Keane et al.[19] found that intraoperative ES induced M2 polarisation and promoted axon elongation. Similar findings were noted in wound healing,[20, 21] limb amputation[22] and amyotrophy.[23] However, the mechanisms via which ES coordinates macrophage polarisation have yet to be fully established.

The ES of nerves is limited by electric burns and mechanical irritation by electrodes.[24] The dielectric material dispersed the quantity of electric charge and reduced the stress, making it a main research direction. The nerve guide conduits made of natural or synthetic biopolymers such as chitosan, gelatin, collagen, polylactide, poly(lactic-co-glycolic acid) or polycaprolactone (PCL) offer supportive mechanical and biochemical cues for nerve regeneration, which can be chaperoned by conductive materials such as polypyrrole (PPy),[17] polyaniline,[25] carbon nanotube[26-28] or reduced-graphene oxide.[29, 30]

We electrospun the PCL and silk fibroin (SF) membrane and coated it with PPy via in situ polymerisation. The compound scaffold, which exhibited electrical conductivity, was used for ES on crushed sacral nerve. We observed accelerated nerve regeneration and alleviated the neurogenic bladder through regulation of macrophage polarisation in the early regenerative microenvironment. High-throughput sequencing presented that signal transducer and activator of transcription (STAT) expression was adjusted in variation which determined the differential responses of macrophages to pro-inflammatory or pro-regenerative signals.

Methods

Fabrication of the PCL/SF membrane and pyrrole polymerisation

PCL/SF membranes were electrospun as described in our previous study[31] with some modification. The PCL pellets (average M_n 80,000, 440744, Sigma-Aldrich, St. Louis, MO, USA) and SF powder (particle size 5 μm, MB4792, Meilunbio, Cambridge, MA, USA) were separately diluted to 8% (w/v) in hexafluoroisopropanol (H1-7501, Aladdin, Shanghai, China), and stirred overnight. The electrospun solutions of PCL and SF were mixed in different ratios and loaded to the mechanical arm connecting positive high voltage. The mixed PCL/SF solutions with positive charges were poured on the negatively charged roller at a rotating speed of 2800 r/min to produce the PCL/SF fibre. The air-dried membranes (2 cm × 2 cm) were immersed in pyrrole (2.5 mM, 8.07492, Sigma-Aldrich) and supplemented with sodium p-toluenesulfonate (2.5 mM, 152536, Sigma-Aldrich). After 2 hours of shaking on ice, they were supplemented with iron chloride (3 mM, dissolved in 1% HCl, I112064, Aladdin) to induce polymerisation under shaking for 6 hours to fully deposit the PPy.[32-34] The membrane was rinsed in distillation-distillation H_2O (ddH_2O) until impurities became invisible, and sterilised with ^{60}Co exposure.

Characterisation of PPy-coated PCL/SF membrane

Scanning electron microscopy images were obtained by field-emission scanning electron microscopy (Quanta FEG 250, ThermoFisher Scientific, Waltham, MA, USA) at an acceleration voltage of 20 kV.[35] Fibre diameters were determined using ImageJ (v1.53t, modded with DiameterJ as previously described).[17]

Fourier transform infrared spectroscopy spectra were recorded on a Nicolet iS50 series (ThermoFisher Scientific) in the region of 4000–400 cm^{-1} using KBr pellets (P116274, Aladdin).

1 School of Medicine, Nankai University, Tianjin, China; 2 Department of Neurosurgery, Chinese PLA General Hospital, Beijing, China; 3 Institute of Orthopedics, Chinese PLA General Hospital; Beijing Key Lab of Regenerative Medicine in Orthopedics; Key Laboratory of Musculoskeletal Trauma & War Injuries PLA; Beijing, China; 4 Co-innovation Center of Neuroregeneration; Nantong University, Nantong, Jiangsu Province, China; 5 Graduate School of Chinese PLA General Hospital, Beijing, China; 6 Department of Ultrasound, Chinese PLA General Hospital, Beijing, China

***Corresponding authors:**
Aijia Shang, shangaj@126.com; Jiang Peng, pengjiang301@126.com; Yu Wang, wangwangdian628@126.com.

#Author equally.

Electrical conductivity of PPy-coated PCL/SF or uncoated PCL/SF was measured by four-probe (RTS-8, 4 Probes Tech, Guangzhou, China) at room temperature.[36] Conductivity was determined using the Van der Pauw equation.

Tensile mechanical properties of PPy-coated PCL/SF were tested on the low-load tensor (C610M, Labthink, Jinan, China) at room temperature.[17] Equal lengths of the prepared membranes were clamped at both ends. The constant crosshead speed was set to 10 mm/min to determine the stress–strain curve under tensile test.[17]

For the biodegradability, samples were soaked in DMEM (11965092, Gibco, Waltham, MA, USA) and incubated at 37°C in a 5% CO_2 atmosphere. The dry weight of samples was tested every day. The biosafety properties of PPy-coated PCL/SF on RAW264.7 macrophages (American Type Culture Collection, Manassas, VA, USA, RRID: CVCL_0493), RSC96 Schwann cells (Bioresource Collection and Research Center, Hsinchu, China, Cat# 60507, RRID: CVCL_4694) and ND27 neurons (European Collection of Authenticated Cell Cultures, Salisbury, UK, Cat# 92090912, RRID: CVCL_4257) were determined via the cell counting kit-8 (CCK-8) assay (CA1210, Solarbio, Beijing, China), PrestoBlue™ Cell Viability Reagent (A13262, Invitrogen, Waltham, MA, USA) and lived/dead cytometry assay (L3224, Invitrogen), as instructed by the manufacturers. We implanted the PPy-coated PCL/SF at lower back subcutaneously and examined the muscles next to the films 7 days later with haematoxylin & eosin staining.

Animal surgery and *in vivo* ES

All animal experiments were in accordance with the Guide for the Care and Use of Laboratory Animals.[37] The Administration Committee of Experimental Animals, the Chinese PLA General Hospital, China approved the use of animals in this study (approval No. 2016-x9-07).

The urethra of females is straighter and shorter, making it easier for urodynamic testing. Therefore, 8–week-old female Sprague-Dawley rats were acquired from Spfbiotech (Beijing, China; license No. SCXK (Jing) 2024-0001) and anaesthetised by intraperitoneal injection of pentobarbital sodium (0.9%, 4 g/kg, P3761, Sigma-Aldrich). The rats were then randomised into sham, crush, scaffold and ES (with scaffold) groups, with six rats in each group. Sham rats received sacral laminectomies and laparotomy of sacral nerves without further crush, while the rats of crush groups received the same surgery and crush as follows: bilateral 2nd sacral laminectomies were performed under the posterior incision to expose the trunk and the root of the bilateral sacral nerves. Crush injuries of the bilateral sacral nerves were performed twice by a microneedle hold maximally clamping (10 seconds each time with 10-second interval). The rats in scaffold group had crushed nerves wrapped and temporarily implanted with PPy-coated PCL/SF scaffold. The scaffold was longer enough to cover the contact of electrode, which is approximately 6 mm. Moreover, the platinum-iridium electrode (Beijing PINS Medical Co., Ltd., Beijing, China) was fixed using an 8-0 suture material onto scaffold with rats of ES groups. Bilateral ES was conducted as single proximal ES protocol guided (impulse wave of 20 Hz, 100 ns per pulse and 3 V for 1 hour).[16, 38, 39] The membrane was then removed and the skin was sutured. The surgical procedures were depicted in **Figure 1A** and **B**.

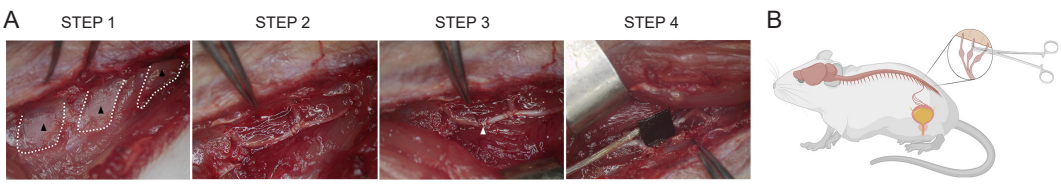

Figure 1. Surgical procedure of sacral nerve crush injury and study design. (A) Surgical procedure with four steps captured under microscope: posterior median approach and excision of S2–S3 vertebral plate (black triangles); dissociation of the sacral nerve and S2–S3 nerve root; crushing of the nerve trunk (white angle) between S2 and S3 nerve root with microneedle holding; wrapping the crushed sacral nerve with PPy-coated PCL/SF membrane and fixation of electrode onto the membrane as well as suture of the membrane. (B) Illustration of the surgical procedure and subsequentneurogenic bladder. Created with BioRender.com. PCL: polycaprolactone; PPy: polypyrrole; SF: silk fibroin.

Rats were housed in the Experimental Animal Center of Chinese PLA General Hospital with free access to water and food. Their bladders were emptied once a day using the crede procedure for 4 weeks until euthanasia using pentobarbital sodium. The investigator was individually blinded to the housed rats as they were unmarked.

Flow cytometry

Sacral nerves were harvested, washed three times with cold phosphate buffer saline (PBS) and transferred into the Hank's balanced salt solution supplemented with collagenase II (0.5 mg/mL, C8490, Solarbio), collagenase II (0.5 mg/mL, C8150, Solarbio) and DNase I (25 μg/mL, D8070, Solarbio) for dissociation. Tissues were cut into pieces and incubated at 37°C for 35 minutes with vortexing every 5 minutes. After filtration, the cell suspensions were centrifuged and incubated with the Zombie Aqua Fixable Viability kit (423102, BioLegend, San Diego, CA, USA) for 15 minutes in the dark. They were washed with PBS, incubated with APC-Cy™7 Anti-RAT CD45 (202216, BioLegend), APC anti-RAT CD86 (200314, BioLegend) as well as FITC anti-RAT CD163 (MCA342F, Bio-Rad, Hercules, CA, USA) and treated with the permeabilization medium (GAS002S100, Invitrogen) for 30 minutes. The cell suspensions were incubated with PE anti-RAT CD68 (MCA341PE, Bio-Rad) for 1 hour in the dark. After repeated washes with PBS, the samples were subjected to flow cytometry (canto II, BD, Franklin Lakes, NJ, USA). All results were analysed using DIVA 8.0 (BD).

Urodynamic test

The retrograde urodynamic test was performed at the end of the observation period as previously described,[2] with some modifications. Briefly, rats were anaesthetised by intraperitoneal injection of urethane (10%, 1 g/kg, 94300, Sigma-Aldrich), the dose of which was adjusted based on toe pinching reflex. A sterile PE-50 catheter was retro-inserted into the bladders through the urethras, after which bladder emptying of was induced by pushing on the abdomen. Then, the bladders were perfused with 0.9% normal saline using an infusion pump (Harvard Apparatus, Holliston, MA, USA) at a rate of 5 mL/h until the first drop of urine could be seen. An electrophysiology recorder (Millar, Houston, TX, USA) with a pressure transducer was connected to PE-50 for cystometrogram with the initial bladder pressure rectified to zero. Urodynamic parameters for each rat (leakage point pressure, and maximum bladder volume) were directly recorded from respective urination cycles. Bladder compliance was calculated as:

$$Bladder\ compliance = \frac{maximum\ bladder\ volume}{leakage\ point\ pressure}$$

High-frequency microultrasoundgraphy

Postvoid residual was measured by a portable digital ultrasound imaging system (Lanmage, Shenzhen, China) to assess urination function. The four groups of rats were anesthetised with inhalational isoflurane (5%, RWD Life Science Co., Shenzhen, China) delivered by a gas anaesthesia machine (Medical Supplies & Services Inc. Ltd., West Yorkshire, UK). Their lower abdomens were shaved with a depilatory paste, covered with the coupling agent (Jinya Co., Tianjin, China) and scanned with a high frequency linear probe (65 channels, 10 MHz, 38 mm). Axial and sagittal section images with the largest areas were acquired. First, the probe was placed in an axial position to capture the oval-shaped bladder and simultaneously measure their widths (D1) and depths (D3). With the probe rotated 90°, wedgy-shaped bladders in the sagittal position were captured and their lengths (D3) measured. Bladder volumes were estimated using the formula:

$$Volume = \frac{D1 \times D2 \times D3}{2}$$

Histopathological evaluation

After experiments, rats were humanely euthanised using overdosed pentobarbital sodium after which the sacral nerves and bladders were harvested. The gross appearance of bladders was imaged. The nerves and bladders were fixed in 4% paraformaldehyde and dehydrated with 30% sucrose solution (powder, S112224, Aladdin). For immunofluorescence, all tissues were embedded in O.C.T Compound (Sakura Tissue Tek, Nagano, Japan) and sectioned into 10 μm using a freezing microtome (CM1950, Leica, Hesse, Germany). For haematoxylin & eosin and Masson's trichrome staining, the tissues were processed by sequential dehydration and waxing using a dehydrator (ASP200S, Leica). The tissues were embedded with an embedding machine (HistoCore Arcadia C, Leica) and sectioned with a pathological microtome (RM2016, Leica). The bladders were stained with a Hematoxylin & Eosin staining kit (G1120, Solarbio) and Masson's trichrome staining kit (G1340, Solarbio). Nerves were stained with Toluidine blue (1%, G3668, Solarbio) for 15 mintes and washed twice. The morphology and distribution of myelin can be observed with confocal scanner. Bladder wall thicknesses were measured after which the ratios of muscles and collagen were calculated using ImageProPlus v6.0 (Media Cybernetics, Rockville, MD, USA). Immunofluorescence staining was conducted as previously described.[31] The slides were incubated in the presence of primary antibodies, including rabbit anti-S100β monoclonal antibody (unconjugated, Clone EP1576Y, 1:200, Abcam, Cat# ab52642, RRID: AB_882426), mouse monoclonal anti-neurofilament 200 (Phos. and Non-Phos.) antibody (1:300, Sigma-Aldrich, Cat# N0142, RRID: AB_477257), rabbit recombinant anti-collagen I antibody [EPR24331-53] (1:400, Abcam, Cat# ab270993, RRID: AB_2927551), mouse anti-collagen III monoclonal antibody (unconjugated, Clone FH-7A, 1:200, Abcam, Cat# ab6310, RRID: AB_305413), mouse CD68 antibody [ED1] (1:400) and CD206/MRC1(E6T5J) XP@ rabbit mAb (1:800). Slides was washed thrice using PBS, incubated with Goat Anti-Rabbit IgG H&L (Alexa Fluor® 594) (1:200, Abcam, Cambridge, UK, Cat# ab150080) and Goat Anti-Mouse IgG H&L (Alexa Fluor 488) preadsorbed Antibody (1:200, Abcam, Cat# ab150117) for 1 hour in the dark, washed three times with PBS, then stained with 4′,6-diamidino-2-phenylindole (DAPI; 1:5000) for 15 minutes, washed three times with PBS and covered with a coverslip. The immunofluorescence images were captured using confocal scanner. All samples were analysed with ImageJ 1.52a.

Isolation and culture of bone marrow-derived macrophages

The isolation and induction of bone marrow-derived macrophages (BMDMs) was performed as previously reported.[40-44] Briefly, cells were rinsed from the femurs of C57BL/6 mice (Spfbiotech) and treated with cold red blood cell lysis buffer (C3702, Beyotime, Shanghai, China) at 4°C for 10 minutes. Resuspended cells were cultured in Dulbecco's modified eagle medium (DMEM; 11965092, Gibco, Waltham, MA, USA), penicillin-streptomycin (5000 U/mL, 15070063, Gibco) and murine macrophage colony-stimulating factor (M-CSF; 10 ng/mL, AF-315-02, Peprotech, Cranbury, NJ, USA). After 6 hours of stationary culture at 37°C in a 5% CO_2 atmosphere, the suspended cells were collected, reseeded into new petri dishes and incubated. The culture medium was refreshed every 3 days. Mature BMDMs were harvested on the 7th day for subsequent assays.

Induction and *in vitro* electrical stimulation of bone marrow-derived macrophages

The BMDMs were seeded in a 12-well plate with PPy-coated PCL/SF membrane and their polarisation towards M1 phenotype induced by lipopolysaccharides (LPS; 100 ng/mL, L8880, Solarbio) and interferon-γ (IFN-γ; 20 ng/mL, P00106, Solarbio) for 24 hours.[45] The home-made platinum electrodes fitting the 12-well plate were sterilised and placed over the plate to make sure the tips were submerged for at least 2 mm. The direct current impulse waves (2.0 V, 20 Hz, 100

μs) for stimulation were generated by connecting the signal generator (DG811, RIGOL, Beijing, China) to the electrode for 1 hour. After 12 hours, the cells were harvested for immunofluorescence staining and quantitative polymerase chain reaction (qPCR) assay.

Immunofluorescence staining

BMDMs were fixed in 4% paraformaldehyde (P1110, Solarbio) for 15 minutes, washed three times with PBS, blocked in 10% normal goat serum (SL038, Solarbio) for 1 hour, incubated overnight at 4°C with mouse CD68 antibody [ED1] (1:500, Abcam, Cat# ab31630, RRID: AB_1141557), CD206/MRC1(E6T5J)XP@ rabbit mAb (1:800, CST, Danvers, MA, USA, Cat# 24595, RRID: AB_2892682), washed three times with PBS, incubated with Goat Anti-Rabbit IgG H&L (Alexa Fluor® 594) (1:200, Abcam, Cat# ab150080, RRID: AB_2650602) and Goat Anti-Mouse IgG H&L (Alexa Fluor 488) preadsorbed Antibody (1:200, Abcam, Cat# ab150117, RRID: AB_2688012) for 1 hour away from light, washed thrice using PBS, then stained with DAPI (1:5000, ab285390, Abcam) for 15 minutes, washed three times with PBS and covered with a coverslip. The immunofluorescence images were captured using confocal scanner (3DHISTECH, Panoramic Confocal, Budapest, Hungary) and the intensity was measured using ImageJ 1.52a.

Quantitative polymerase chain reaction

BMDMs were plated in a petri dish at a density of 5×10^6 cells/mL, induced and electrically stimulated. The total RNA was extracted using the FastPure Total RNA Isolation kit (RC112-01, Vazyme, Nanjing, China). The nucleic acid analyser (NanoDrop2000, ThermoFisher Scientific) was used to assess the RNA concentration, which was normalised to the control group. Reverse transcription was performed using the ReverTra Ace® qPCR RT Kit (FSQ-201, Toyobo, Osaka, Japan) at 37°C for 15 minutes and at 85°C for 5 seconds. The qPCR was performed using the StepOne™ Real-Time PCR System (4376357, Applied Biosystems, Waltham, MA, USA): 95°C for 5 minutes, followed by 40 cycles of 15 seconds at 95°C, and 15 seconds at 65°C. Primer was synthesised by Sangon Biotech (Shanghai, China) and sequences for *Il1b*, *Tnfa*, *Il6*, *Il12*, *Arg1*, *Ym1*, *Retnla*, *Mrc1*, *Stat1*, *Stat3*, *Stat6*, *Jak1*, and *Jak2* are shown in **Table 1**. Relative mRNA expressions were determined by normalising to *β-actin*.

High-throughput sequencing

The BMDMs were lysed with Trizol (15596018, Life Technologies, Waltham, MA, USA) for 10 minutes and snap frozen in liquid nitrogen. Library construction, high-throughput sequencing, as well as data collection and analyses were performed at CapitalBio Technology., Inc. (Beijing, China). Briefly, total RNA was extracted and assessed using the Agilent 2100 BioAnalyzer (Agilent Technologies, Santa Clara, CA, USA) and Qubit Fluorometer (Invitrogen). The RNA-seq libraries of triplicate samples were generated and sequenced by CapitalBio Technology using the NEB Next Ultra RNA library Prep Kit for Illumina. The products were purified and enriched by qPCR to amplify the library DNA, followed by paired-end sequencing with pair end 150-base pair ending length on an Illumina NovaSeq sequencer (Illumina, San Diego, CA, USA). Sequencing qualities were assessed with FastQC (v0.11.5), with reference to the hg38 human genome.[46] Processed reads from each sample were aligned against the reference genome using HISAT2 (v1.3.3b, http://daehwankimlab.github.io/hisat-genotype/). Gene expression analyses were performed using StringTie (v1.3.3b, https://github.com/gpertea/stringtie) while differential expression genes (DEGs) analysis between samples were analysed using DESeq (v1.28.0, https://bioconductor.org/packages/release/bioc/html/DESeq.html). Independent statistical hypothesis testing was separately conducted on DEGs. Then, a *P*-value was obtained, which was corrected by the false discovery rate (FDR) method. The corrected *P*-value (*q*-value) was obtained using the BH method. The *P*- or *q*-values were set as thresholds for significance. The parameters for classifying significantly DEGs were ≥ 2-fold differences (|log2 fold change | ≥ 1) in the transcript abundance and $P \leq 0.05$. Subsequently, Gene Ontology (GO) analysis was based on the DEGs results referring to the GO annotation database (https://www.geneontology.org/).[47-50] With R packages "clusterProfiler (https://github.com/YuLab-SMU/clusterProfiler)", "enrich (https://github.com/wjawaid/enrichR)", "GOplot", "ggplot2"and "org.Hs.e.g.db" used, we explored their enrichment in molecular function, biological processes, and cellular components. Kyoto Encyclopedia of Genes and Genomes (KEGG) enrichment analysis was performed to detect enrichment of pathways between groups with the R "clusterProfiler" package. The Sankey analysis (https://github.com/davidsjoberg/ggsankey) was based on the KEGG analysis and were used to attribute the influence of genes to enrichment of pathway. The STRING database (https://cn.string-db.org/)[51] was used to construct a protein-protein interaction network and revisualised using Cytoscape (v3.7.1). The confidence score of protein interactions was set as > 0.9. A set of hub genes was selected based on the maximal clique centrality algorithm and degree according to CytoHubba (v0.1, https://apps.cytoscape.org/apps/cytohubba).[51]

Statistical analysis

Data are expressed as mean standard error of the mean (SEM), and were analysed using IBM SPSS Statistics for Windows (version 27.0, IBM Corp., Armonk, NY, USA) and GraphPad Prism (version 9.4.0 for Windows, GraphPad Software, Boston, MA, USA, www.graphpad.com). Comparisons of means between two groups were performed using the Student's *t*-test with $P < 0.05$ as the threshold for statistical significance. While some comparisons of means between more than three groups were performed using the one-way analysis of variance followed by Bonferroni's *post hoc* test with $P < 0.0332$ as the threshold for statistical significance.

Results

Construction and characterisation of PPy-coated PCL/SF membrane

Pyrrole was polymerised on surfaces of PCL/SF membranes without significantly changing their flexibility (**Figure 2A** and **B**), morphologies of which were observed and confirmed

Table 1. Primer sequences for quantitative polymerase chain reaction

Gene	Primer sequence (5′ to 3′)
β-Actin	Forward: TCC ATC ATG AAG TGT GAC GT
	Reverse: TAC TCC TGC TTG CTG ATC CAC
Il1b	Forward: TAC GGA CCC CAA AAG ATG A
	Reverse: TGC TGC TGC GAG ATT TGA AG
Tnfa	Forward: ACG GCA TGG ATC TCA AAG AC
	Reverse: AGA TAG CAA ATC GGC TGA CG
Il6	Forward: TAG TCC TTC CTA CCC CAA TTT CC
	Reverse: TTG GTC CTT AGC CAC TCC TTC
Il12	Forward: TCT CAC CGT GCA CAT CCA AG
	Reverse: GCC AAA AAG AGG AGG TAG CGT
Arg1	Forward: CTC CAA GCC AAA GTC CTT AGA G
	Reverse: AGG AGC TGT CAT TAG GGA CAT C
Ym1	Forward: AGA AGG GAG TTT CAA ACC TGG T
	Reverse: GTC TTG CTC ATG TGT GTA AGT GA
Retnla	Forward: CTG GGT TCT CCA CCT CTT CA
	Reverse: TGC TGG GAT GAC TGC TAC TG
Mrc1	Forward: CTC TGT TCA GCT ATT GGA CGC
	Reverse: CGG AAT TTC TGG GAT TCA GCT TC
Stat1	Forward: GCC AGG CTT GGT GAT TGA C
	Reverse: TCA GGA AGA AGG AGA GAT TCC TG
Stat3	Forward: CAC CTT CCT ACT GCG CTT CA
	Reverse: GTA CGG GGC AGC ACT ACC T
Stat6	Forward: TGG TCG GTT CAG ATG CTT TC
	Reverse: AGG TGG CGG AAC TCT TCT A
Jak1	Forward: TGA CCA GGC AAG ATC CAG A
	Reverse: AAG TCC CGG TGA ACG TAT TG
Jak2	Forward: TCG CCG GCC AAT GTT CT
	Reverse: ACA CAG GCG TAA TAC CAC AAG

Note: Arg1: arginase 1; Il12: interleukin 12; Il1b : interleukin 1 beta; Il6: interleukin 6; Jak1/2: Janus kinase 1/2; Mrc1: mannose receptor, c type 1; Retnla: resistin-like alpha; Stat1/3/6: signal transducer and activator of transcription 1/3/6; Tnfa: tumour necrotic factor alpha.

by scanning electron microscopy. The granular process above the PCL/SF fibres indicated the appropriate extent of the reaction. There was no excess polymer that may have dissociated and damaged the resident microenvironment. Fourier transform infrared spectroscopy was also performed (**Figure 2C**). Addition of PPy resulted in higher stress levels than the PCL/SF membrane, which could reach the 11.151 MPa, improving the mechanical property of the membrane (**Figure 2D**). Conductivity, which was measured by the four-probes revealed significant increases after coating of the PPy (2.4127 ± 0.4989 S/cm; **Figure 2E**), compared to the uncoated PCL/SF of conductivity lower than the limit of detection. The scanning electron microscopy images showed that the radius of fibre was in the range of 0.1 to 0.15 μm (**Figure 2F**). The CCK-8 assay, PrestoBlue assay and live/dead cytometry with three major cell types (ND27, RSC96, and RAW264.7 cells) did not reveal significant differences in cell toxicity among all groups (**Figure 2G–J**). And we found no evidence of necrosis when attached the membrane on rat muscles over 7 days (**Figure 2K**). In summary, we have constructed a PPy-coated PCL/SF membrane with favourable mechanical, electrical and biological properties for further applications in nerve injury.

PPy-coated PCL/SF with ES promotes sacral nerve regeneration after crush injury

To investigate the effects of PPy-PCL/SF scaffold and ES, we crushed the sacral nerves at the S2 level and encircled the injured nerves with the scaffold. The rats with crushed sacral nerves were subjected to 1 hour of localised ES after wrapping, parameters of which were determined as previously described[2,31] (**Figure 1A**). At 28 days after surgery, nerves and bladders were harvested and assessed. The neurofilament 200-positive nerve fibres were degenerated and reduced after injury, which was indicated by the intensity ($t_{(20)}$ = 2.771, P = 0.0035 < 0.05) and number of neurofilament 200-positive fibres ($t_{(20)}$ = 5.479, P < 0.0001; **Figure 3A–D** and **F**). The PPy-PCL/SF did not exhibit the regenerative effects (intensity: $t_{(20)}$ = 0.7191, P = 0.8597 > 0.05; number: $t_{(20)}$ = 0.3713, P = 0.9767 > 0.05). ES promoted axon regeneration (intensity: $t_{(20)}$ = 4.836, P = 0.0003 < 0.001; number: $t_{(20)}$ = 2.940, P = 0.0241 < 0.05). Axon myelination by Schwann cells is crucial for peripheral nerve regeneration. The intensity and number of S100β revealed the Schwann cells were severelydamaged and their abundance was significantly decreased after acute injury (intensity: $t_{(20)}$ = 2.665, P = 0.0440 < 0.05; number: $t_{(20)}$ = 4.155, P = 0.0015 < 0.01). The situation of

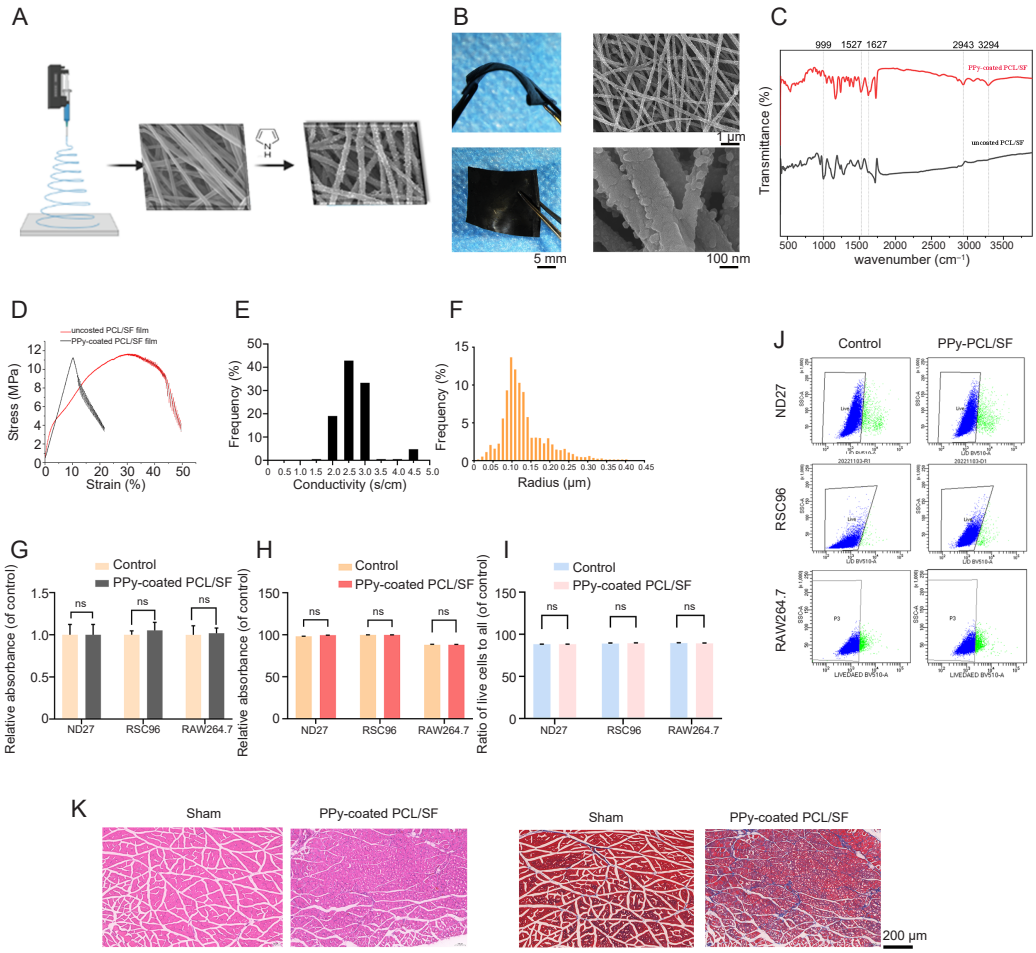

Figure 2. Construction and characterisation of PPy-coated PCL/SF membrane. (A) The schematic diagram of the electrospun PCL/SF fibres and in situ polymerisation of pyrrole. (B) Representative PPy-coated PCL/SF membrane (left panel) and surface morphology observed with scanning electron microscopy (right panel). Scale bars: 5 mm (left), 1 μm (upper right), and 100 nm (lower right). (C) Transmittances of uncoated PCL/SF membrane and PPy-coated PCL/SF membrane detected by Fourier transform infrared spectroscopy, marked with characteristic absorption peak. (D) The stress-strain curves tested with low-load tensile machines. (E, F) The conductivity (E) and radius (F) distribution of PPy-coated PCL/SF membrane. (G, H) The cell viability of ND27, RSC96 and RAW264.7 cells tested with CCK-8 assay (G) and PrestoBlue assay (H). (I, J) The cell viability ofND27, RSC96 and RAW264.7 cells measured with live/dead assay. (K) The haematoxylin & eosin staining (left panel) and Masson's trichrome staining (right panel) of muscles received transplantation of PPy-coated PCL/SF membranes or control. Scale bar: 200 μm. Data are shown in mean ± SEM (n = 3 per group), and were analysed by Student's t-test. CCK-8: cell counting kit-8; ns: not significant; PCL: polycaprolactone; PPy: polypyrrole; SF: silk fibroin.

Schwann cells was not improved by application of PPy-coated PCL/SF membrane (intensity: $t_{(20)} = 0.4982$, $P = 0.9467 > 0.05$; number: $t_{(20)} = 0.08785$, $P = 0.9997 > 0.05$), but did not rescued by ES (intensity: $t_{(20)} = 2.877$, $P = 0.0277 < 0.05$; number: $t_{(20)} = 3.258$, $P = 0.0118 < 0.05$; **Figure 3A**, **E** and **G**).

Toluidine blue staining was performed to assess the microcosmic changes of the axon and myelin. There was myelin regression and loss to varying degrees in the crush and PPy-PCL/SF groups, compared with the ES group (**Figure 3B**). Transmission electron microscopy revealed significant differences in myelin thickness (Crush *vs.* Sham: $t_{(20)} = 3.811$, $P = 0.0033 < 0.01$; Scaffold *vs.* Crush: $t_{(20)} = 0.9993$, $P > 0.05$; ES *vs.* Scaffold: $t_{(20)} = 2.988$, $P = 0.0217 < 0.05$; **Figure 3C** and **H**). Those results demonstrated the neuroprotective effect of single immediate ES after crush injuries as presented results of the improved demyelination and promoted axon regeneration. According to Maeng et al.'s review,[52] we believed with affirmation that the ES played a role of pro-regeneration through shaping the post-injured microenvironment once for all. It awaited us to determine whether macrophages are engaged in the ES-induced regeneration promotion.

PPy-coated PCL/SF with ES improves neurogenic bladder symptoms and histological lesions

As one of the major important target organs of the sacral nerve, the bladder is susceptible to all types of sacral nerve injury and exhibits various symptoms referred to neurogenic bladder. In

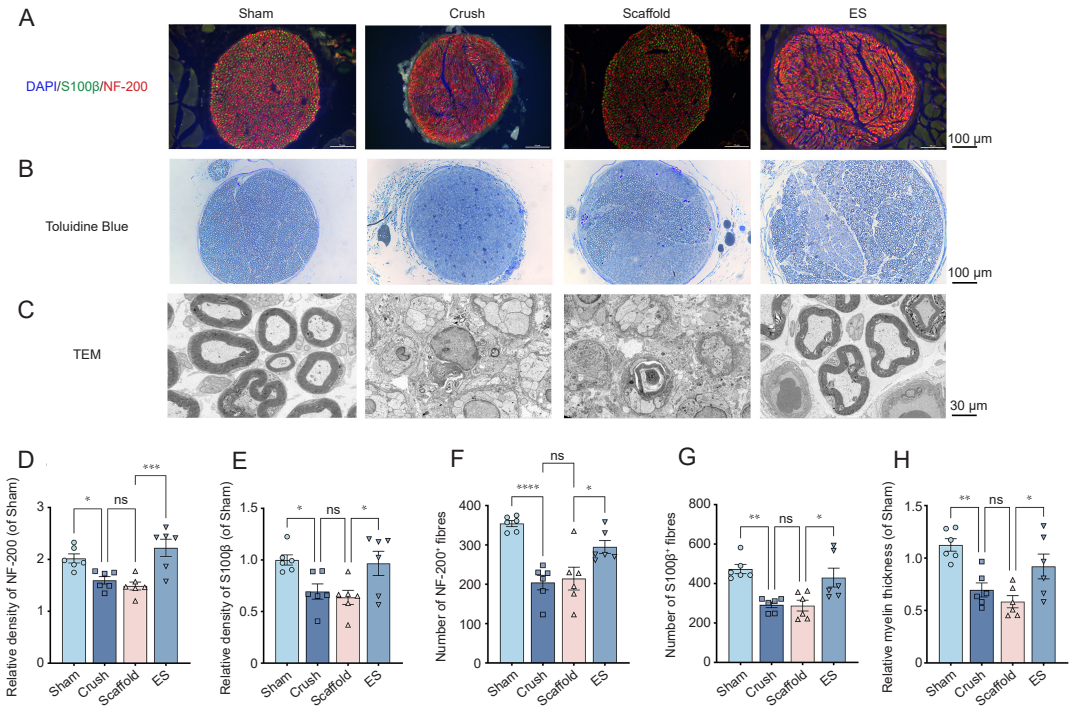

Figure 3. PPy-coated PCL/SF with ES promoted promotes sacral nerve regeneration at 28 days post-injury. (A) Representative fluorescence images of S100β (Alexa Fluor 488) and NF-200 (Alexa Fluor® 594) in crushed sites. Scale bar: 100 μm. (B) Representative images of toluidine blue staining. Scale bar: 100 μm. (C) Representative TEM-captured images. Scale bar: 30 μm. (D, E) The semi-quantification of fluorescent intensity of NF-200 (D) and S100β (E). (F, G) Quantification of NF-200-positive nerve fibres (F) and S100β-positive cells (G). (H) Quantification of myelin thickness measured by transmission electron microscopy. All data are shown as mean ± SEM ($n = 6$ per group). *$P < 0.05$, **$P < 0.01$, ***$P < 0.001$, ****$P < 0.0001$ (one-way analysis of variance followed by Bonferroni's *post hoc* test). DAPI: 4′,6-diamidino-2-phenylindole; ES: electrical stimulation; NF-200: neurofilament 200; TEM: transmission electron microscopy.

Figure 4A, there was swelling and expanding of the bladder, which was alleviated by ES treatment. To investigate the bladder protective effects of ES, haematoxylin & eosin staining was performed to measure bladder thickness (Crush *vs.* Sham: $t_{(20)} = 10.54$, $P < 0.0001$; Scaffold *vs.* Crush: $t_{(20)} = 3.335$, $P = 0.0099 < 0.01$; ES *vs.* Scaffold: $t_{(20)} = 3.553$, $P = 0.0030 < 0.01$; **Figure 4A**, **B** and **G**). The significant changes in thickness were attributed to enlargement of interstitial spaces and abnormal collagen hyperplasia that superseded the atrophic muscles, especially the detrusor, which was confirmed by Masson's trichrome staining. The muscle and collagen areas were measured (Crush *vs.* Sham: $t_{(20)} = 10.59$, $P < 0.0001$; Scaffold *vs.* Sham: $t_{(20)} = 1.373$, $P = 0.4589 > 0.05$; ES *vs.* Scaffold: $t_{(20)} = 6.881$, $P < 0.0001$; **Figure 4C** and **H**). Higher magnification revealed bladder wall vasodilation and inflammation in the crush and scaffold groups. Accompanied by increased collagen levels, there was a switch from collagen 3 to collagen 1 using immunofluorescence as showed in **Figure 4D** and **I**.

The urodynamic test was performed to assess denervation of the detrusor and atrophy of smooth muscles. The urodynamic curve revealed a smoothly ascending slope and prolonged urination latency in the crush group, compared to the Sham groups, indicating damaged contractability of detrusor and diastolic functions of smooth muscles. There were significant differences in leakage point pressure, while the calculated bladder compliance revealed that it was more sensitive to bladder dysfunctions caused by sacral nerve injury (Crush *vs.* Sham: $t_{(20)} = 8.239$, $P = 0.0095 < 0.01$; ES *vs.* Scaffold: $t_{(20)} = 4.360$, $P = 0.0491 < 0.05$; **Figure 4E, J**, and **K**). Thus, uroschesis can be detected by ultrasound and the bladder volume calculated (Crush *vs.* Sham: $t_{(20)} = 5.754$, $P < 0.0001$; ES *vs.* Scaffold: $t_{(20)} = 2.790$, $P = 0.0335 < 0.05$; **Figure 4F**, and **L**). Taken together with all the above results, we found that ES with crushed sacral nerves could alleviate the neurogenic bladder symptoms and decrease the histological change compared to the crush groups.

Treatment of macrophages with ES promotes their polarisation from LPS/IFN-γ-induced M1 to M2

As important coordinators of the microenvironment, macrophages have bidirectional effects: pro-inflammation and pro-regeneration.[9, 11] The timing of macrophage polarisation shift, if delayed, can cause excess inflammation and suppress nerve regeneration. There is a need to determine whether ES promotes nerve regeneration by regulating macrophages. We isolated the BMDMs and co-cultured them with the PPy-PCL/SF scaffold. Then, the BMDMs were subjected to ES at the same parameters as *in vivo*. Cells expressing CD68 occupying most view showed **Figure 3A**, indicating a purity of BMDMs. Next, we found no significant difference of CD206/CD68 ratio between control and PPy groups ($t_{(8)} = 0.3736$, $P = 0.9777 >$

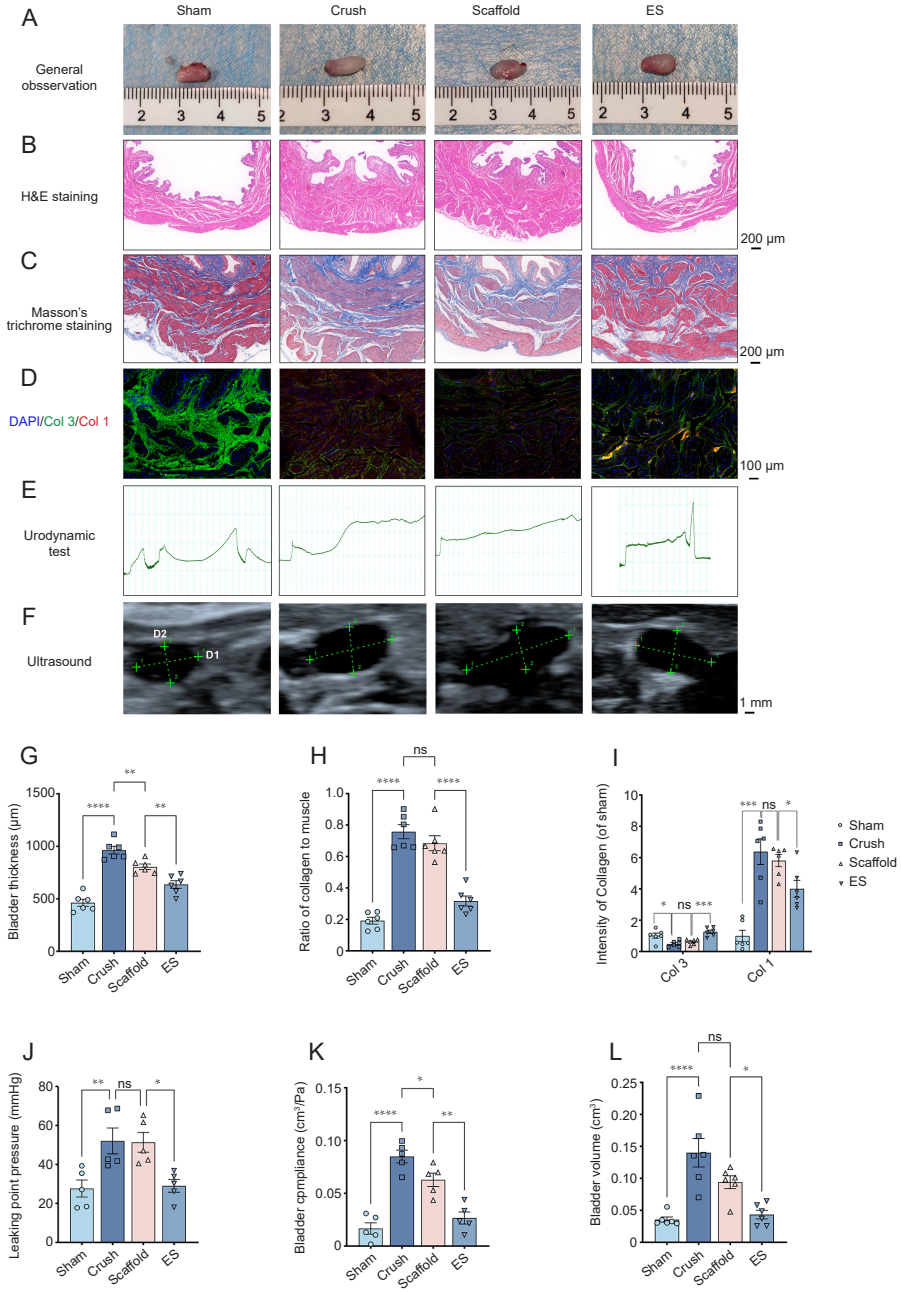

Figure 4. PPy-coated PCL/SF with ES improves neurogenic bladder symptoms and histological lesions at 28-days post-injury. (A) Representative images of bladder in general observation. (B) Representative images of haematoxylin & eosin staining. Scale bar: 200 μm. (C) Representative images of Masson's trichrome staining in bladder. The muscle was stained as red while collagen was stained as blue. Scale bar: 200 μm. (D) Representative fluorescent images of Col 3 (green, Alexa Fluor 488) and Col 1 (red, Alexa Fluor® 594) in bladder. Scale bar: 100 μm. (E) Representative urodynamic curves. (F) Representative ultrasonic images. The width was marked as D1 and depth was marked as D2. Scale bar: 1 mm. (G) Bladder thickness measured with haematoxylin & eosin staining. (H) Ratio of collagen to muscle measured with Masson's trichrome staining. (I) The density of Col 3 and Col 1 in all groups. (J–L) Leaking point pressure (J), bladder compliance (K) and bladder volume (L) in urodynamic test. Data are shown as mean ± SEM ($n = 6$ per group). *$P < 0.05$, **$P < 0.01$, ***$P < 0.001$, ****$P < 0.0001$ (one-way analysis of variance followed by Bonferroni's *post hoc* test). Col 1: collagen I; Col 3: collagen III; DAPI: 4′,6-diamidino-2-phenylindole; ES: electrical stimulation; H&E: hematoxylin-eosin; ns: not significant; PCL: polycaprolactone; PPy: polypyrrole; SF: silk fibroin.

0.05), which showed PPy-coated PCL/SF membrane could not altered the polarisation. While significant differences in the ratio of CD206/CD68 intensity were noted (PPy + LPS/IFN-γ *vs.* PPy: $t_{(8)} = 3.423$, $P = 0.0269 < 0.05$; PPy + LPS/IFN-γ+ ES *vs.* PPy + LPS/IFN-γ: $t_{(8)} = 13.35$, $P < 0.0001$; **Figure 5A** and **E**). The *in vitro* result may not reflect the fate of macrophage of neural regeneration microenvironment. Therefore, we examined the *in vivo* macrophage polarisation with immunofluorescent staining which showed $CD68^{+}CD206^{+}$ macrophage concentrated most in ES group as showed in

Figure 5C. Quantitative analysis of flow cytometry confirmed the results. The ratio of $CD45^+CD68^+CD86^+CD163^+$ cells to $CD45^+CD68^+CD86^-CD163^-$ cells was decreased ($t_{(6)} = 7.543$, $P = 0.0017 < 0.05$), but increased after ES ($t_{(6)} = 5.820$, $P = 0.0023 < 0.05$; **Figure 5B** and **D**).

On the transcriptional level, the ES suppressed the expressions of M1-related markers (*Il1b*: $t_{(4)} = 3.197$, $P = 0.0330 < 0.05$; *Il6*: $t_{(4)} = 4.024$, $P = 0.0158 < 0.05$; *Il12*: $t_{(4)} = 5.636$, $P = 0.0049 < 0.01$; *Tnfa*: $t_{(4)} = 4.936$, $P = 0.0078 < 0.01$; **Figure 5F–I**). Expressions of the M2-assciated genes were significantly upregulated (*Arg1*: $t_{(4)} = 3.780$, $P = 0.0194 < 0.05$; *Mrc1*: $t_{(4)} = 28.26$, $P < 0.0001$; *Retnla*: $t_{(4)} = 2.942$, $P = 0.0423 < 0.05$; *Ym1*: $t_{(4)} = 3.011$, $P = 0.0395 < 0.05$; **Figure 5F–M**).

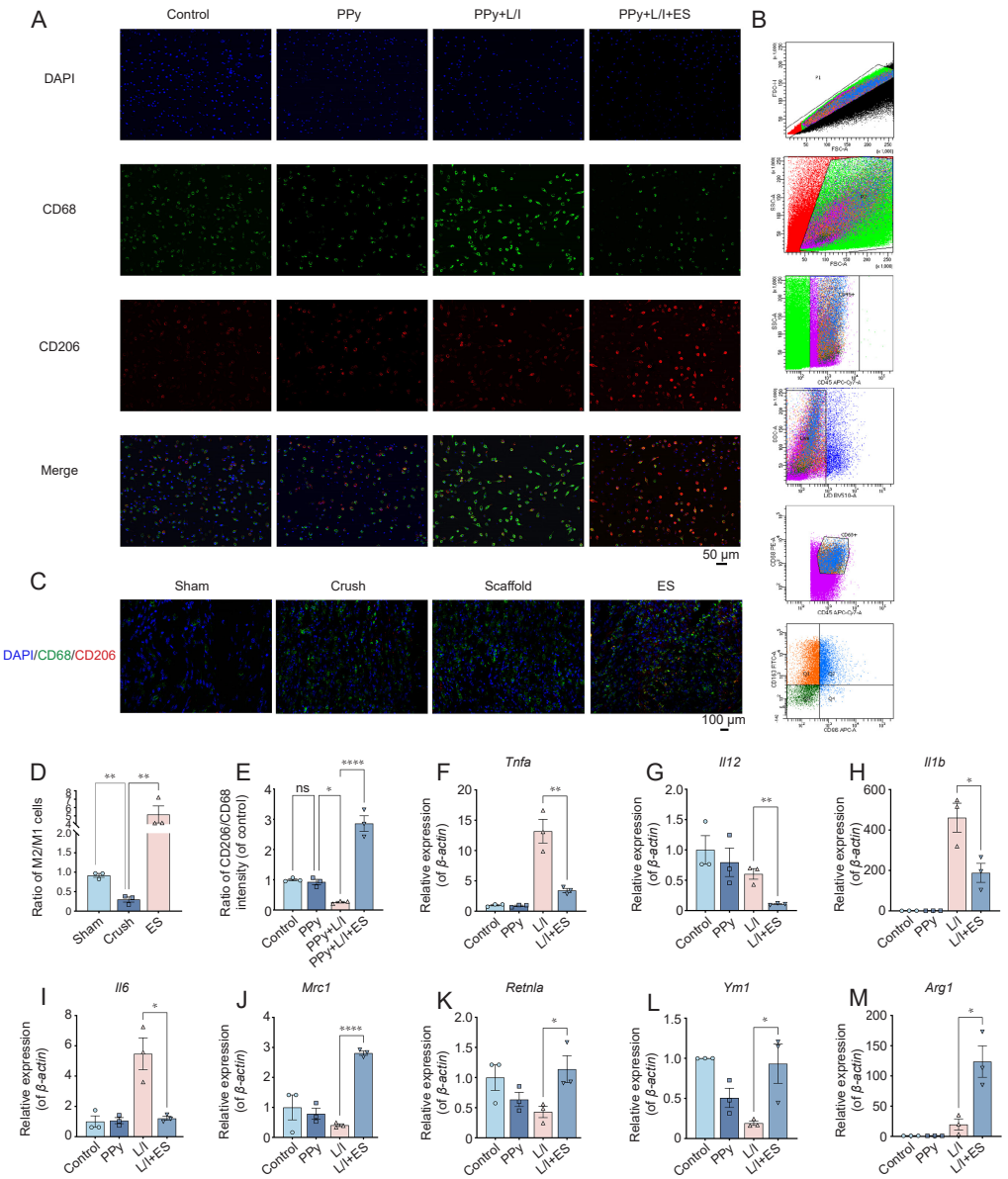

Figure 5. Determination of macrophage polarisation. (A) Representative fluorescence images of CD68 (green, Alexa Fluor 488) and CD206 (red, Alexa Fluor® 594) in BMDMs. Scale bar: 50 μm. (B) The representative scatter plot of $CD45^+CD68^+CD163^{Hi}CD86^{Low}$ cells and $CD45^+CD68^+CD163^{Low}CD86^{Hi}$ cells using flow cytometry. The cells were harvested from sacral nerves of four groups at 7-day post-injury. (C) The representative images of $CD68^+CD206^-$ cells and $CD68^+CD206^+$ cells in rats at 7-day post-injury. Scale bar: 100 μm. (D) The ratio of M2 macrophages ($CD45^+CD68^+CD163^{Hi}CD86^{Low}$ cells) to M1 macrophages ($CD45^+CD68^+CD163^{Low}CD86^{Hi}$ cells) in flow cytometry presented in B. (E) Semi-quantification of immunofluorescence intensity of CD206 to CD68. (F–M) Relative mRNA expression of M1-related marker and M2-related marker. Data are shown as mean ± SEM ($n = 3$ per group). $^*P < 0.005$, $^{**}P < 0.01$, $^{****}P < 0.0001$ (one-way analysis of variance followed by Bonferroni's *post hoc* test). Arg1: arginase 1; BMDM: bone marrow-derived macrophage; DAPI: 4′,6-diamidino-2-phenylindole; ES: electrical stimulation; Il12: interleukin 12; Il1b : interleukin 1 beta; Il6: interleukin 6; Jak1: Janus kinase 1; Jak2: Janus kinase 2; L/I: lipopolysaccharides/interferon-γ; Mrc1: mannose receptor, c type 1; ns: not significant; PPy: polypyrrole; Retnla: resistin-like alpha; Stat1: signal transducer and activator of transcription 1; Stat3: signal transducer and activator of transcription 3; Stat6: signal transducer and activator of transcription 6; Tnfa: tumour necrotic factor alpha.

Electrical stimulation regulates macrophage polarisation via the JAK-STAT signalling pathway

Studies have aimed at assessing the mechanisms of ES in regulating cell fates. The macrophages exhibiting unique responsiveness to multiple stimuli are activated by different mechanisms that have not been fully established. We comprehensively analysed the gene expression profiles by high-throughput RNA sequencing in non-induced BMDMs (M0), LPS/IFN-γ-induced BMDMs (LPS/IFN-γ) and ES + LPS/IFN-γ induced BMDMs (ES) groups. In **Figure 6A**, a total of 4557 genes were found to be differentially expressed between the ES + LPS/IFN-γ groups, among which 1178 genes were significantly changed after LPS/IFN-γ treatment, compared with the M0 group. The DEG analysis revealed that the most down-regulated genes in the ES groups were chemokine-related (*Ccl5*, *Irf7*, *Cxcl10*, *Ifit1* and *Il1b*),[53-55] indicating that cascade amplification of inflammation by macrophages was blocked after ES (**Figure 6B**). The potential of Anxa856 for enhancing M2 polarisation has been reported while the neurotrophic factors (*Ngf*, *Nrep* and *Edil3*)[57, 58] facilitate axon regeneration. The Fn1 encode fibronectin1, which makes up the basal structure of nerve outgrowth.[59] Thus, after ES, gene expressions of macrophages were alternated to M2 profiles. The genes encoding the voltage-gated channels (*Cacnb1*, *Cacng7*, *Clcn7* and *Prap1*) were differentially expressed, and are important in ES-induced transcriptional changes.

GO analysis showed that the biological process was enriched in immunological response and inflammation as a cascade of cytokines and chemokines was differentially regulated (**Figure 6C**). The extracellular organelle and extracellular membrane-bound organelle were significantly changed, indicating the activation of infiltration. The focal adhesion was also altered. The extracellular vesicle and extracellular exosome which were enriched may implied the activation of secretion of EVs. For the molecular function, some metabolite binding was significantly regulated, for example, anion, carbohydrate derivative and nucleoside. It is usually speculated that those terms correlated with transcriptional regulation.

Enrichment analysis was performed to identify the significantly differentially enriched pathways between the ES and LPS/IFN-γ groups using the KEGG database (**Figure 6D**). The adenosine 5′-monophosphate-activated protein kinase (AMPK) signalling pathway,[60] peroxisome proliferators-activated receptor (PPAR) signalling pathway,[10, 61] JAK-STAT signalling pathway[62] and PI3K-Akt signalling pathway[63] are of intermediate importance in macrophage polarisation. The cytokine-cytokine receptor interaction pathway and chemokine signalling pathway were significantly enriched, however, most of which were downstream proteins regulated by the signal transduction harmonised between the ES and pro-inflammation stimuli. The calcium signalling pathway exhibited unique intermediate effects between the ES effects and transcriptional regulation.[64, 65]

The traditional KEGG visualised analysis may not have assessed the impact of the most variably expressed genes in KEGG pathways, therefore, Sankey analysis, which focuses on the most significantly expressed genes and pathways, was performed. The nerve growth factor (NGF) signalling was upregulated, with genes such as *Mapkapk2*,[66] *Fgfr1*,[67] *Src*[68] and *Csf3r* that are favourable for wound healing. The *Col1a2*,[69] *Mmp14*,[70] *Sdc1* and *Sdc3* were highly correlated with extracellular matrix organisation by macrophages, which may have an important role in nerve regeneration.[71] Besides, macrophages coordinate foreign body reactions via the pathway to promote "scar-like" tissue formation while also resolving inflammation by accelerating the formation of connective tissues to bridge the minor gaps.[72] Platelet activation promotes regeneration via release of platelet granules, leading to endothelial activation and growth factor secretion.

The protein-protein interaction network was constructed and the hub genes identified. In **Figure 6E** and **F**, *Stat1* was modulated by ES. Zhang et al.[73] reported that there are four JAKs and seven STATs mediating the transduction of almost 60 cytokines, hormones and growth factors. Homodimers of JAKs can phosphorylate themselves in response to cytokine binding and pass the phosphates to STATs to become dimers and move intranuclearly to activate target gene transcriptions. Canonical JAKs and STATs are highly selective. The STAT1 and STAT3 transduce pro-inflammation signals like IFN-γ, while STAT6 transduce pro-regeneration signals.[62, 73, 74] The qPCR results indicated that *Stat1* ($t_{(4)}$ = 3.359, P = 0.0283 < 0.05), *Stat3* ($t_{(4)}$ = 4.523, P = 0.0106 < 0.05) were down-regulated while *Stat6* ($t_{(4)}$ = 9.603, P = 0.0007 < 0.001) expressions were up-regulated. However, *Jak1* ($t_{(4)}$ = 0.9585, P = 0.3921 > 0.05) and *Jak2* ($t_{(4)}$ = 0.7565, P = 0.9433 > 0.05) expressions were not affected, as showed in **Additional Figure 1A**. In the meantime, we found a significant increase of intracellular calcium concentration after ES ($t_{(4)}$ = 7.990, P = 0.0013 < 0.05) , which agreed with the up-regulated genes that encoded calcium channel substrate. However, the mechanism on the calcium regulating STATs transcription was still hidden in the mist.

Electrical stimulation-manipulated macrophage promotes sacral nerve regeneration

As the ES may post paradox impacts on various component besides macrophage, we performed ES-manipulated macrophage transplantation experiments after crush injury as described above (**Figure 7A**) and observed improved nerve regeneration. The intensity of S100β ($t_{(8)}$ = 3.074, P = 0.0153 < 0.05) and neurofilament 200 ($t_{(8)}$ = 1.698, P = 0.1279 > 0.05) was mildly changed with replantation of non-treated BMDMs compared to those crushed (**Figure 7B**, **C** and **E**). It was even worse for those transplanted with LPS/IFN-γ induced BMDMs (S100β: $t_{(8)}$ = 3.556, P = 0.0074 < 0.01; neurofilament 200: $t_{(8)}$ = 2.378, P = 0.0447 < 0.05) , however, better for those with macrophage induced by ES and LPS/IFN-γ (S100β: $t_{(8)}$ = 3.827, P = 0.0050 < 0.01; neurofilament 200: $t_{(8)}$ = 3.699, P = 0.0061 < 0.01). Then, we evaluated the histological reconstruction of neurogenic bladder. The Masson's trichrome staining showed the ratio of collagen to muscle was unchanged when transplanted with BMDMs without induction ($t_{(8)}$ = 0.6957, P = 0.5063 > 0.05; **Figure 7D** and **F**). The significant increase was found in BMDMs (LPS/IFN-γ) group ($t_{(8)}$ = 2.689, P = 0.0275 < 0.05). However, electrically stimulated BMDMs remodeled the neurogenic bladder

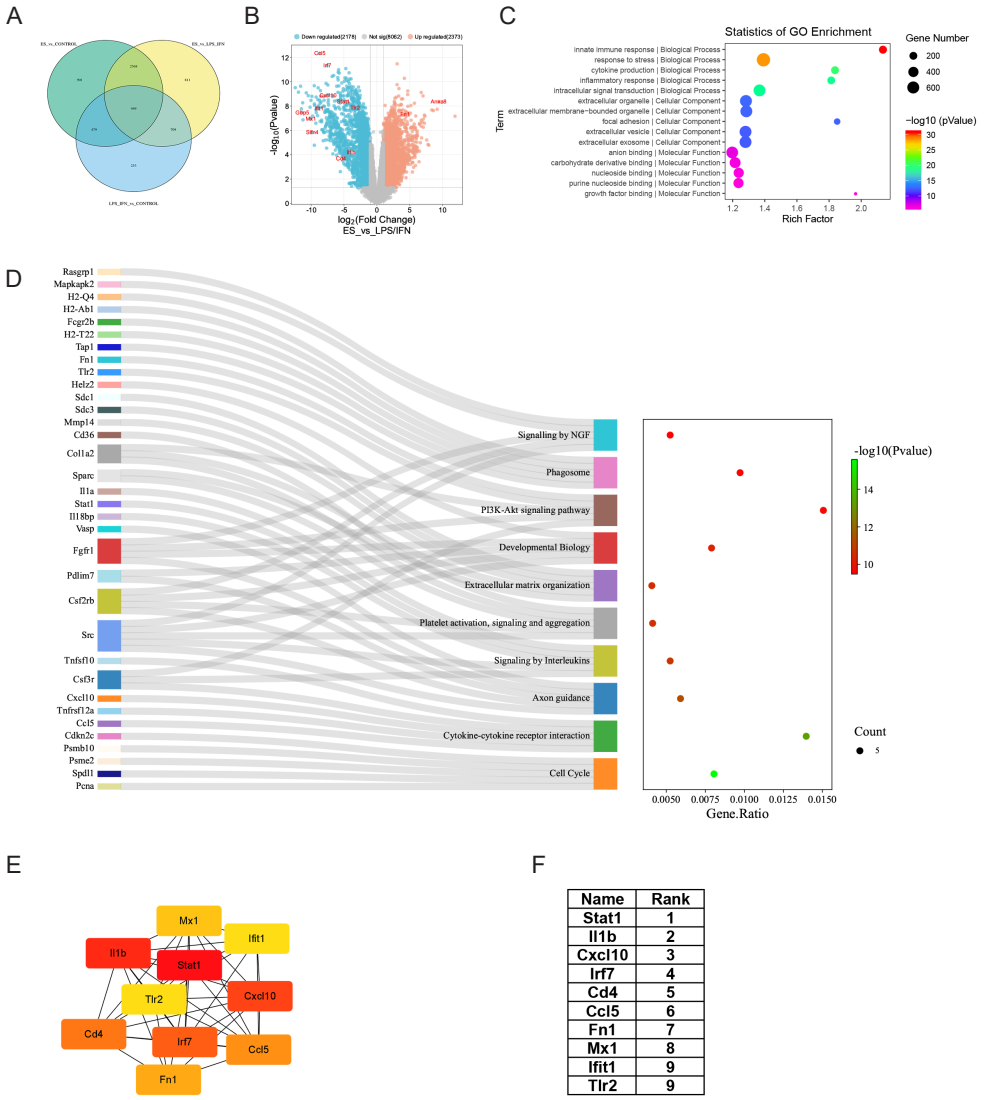

Name	Rank
Stat1	1
Il1b	2
Cxcl10	3
Irf7	4
Cd4	5
Ccl5	6
Fn1	7
Mx1	8
Ifit1	9
Tlr2	9

Figure 6. The high-throughput sequencing analysis of BMDMs with LPS/IFN-γ induction and ES treatment. (A) Venn plot illustrated the differentially expressed genes between Control (non-treated BMDMs) and LPS/IFN-γ (BMDMs with LPS/IFN-γ induction) groups, Control and ES (BMDMs with LPS/IFN-γinduction and ES treatment), ES and LPS/IFN-γ. (B) Volcanic plot showed the up-regulated and down regulated genes between ES and LPS/IFN-γ. The genes with adjust. $P < 0.05$ and |log2 fold change | ≥ 1 were considered significantly changed. The top 20 genes with most significant fold change was marked in red. (C) The heatmap illustrated five most enriched GO terms in BP, CC and MF. (D) The contribution of differentially expressed genes to KEGG terms enrichment was displayed separately with Sankey analysis, as the KEGG terms with $P < 0.05$ were considered as significantly enriched. (E, F) Protein-protein interaction network included 10 genes was generated using method of degree and the rank was list in F. BMDM: bone marrow-derived macrophage; BP: biological process; CC: cellular component; ES: electrical stimulation; GO: Gene Ontology; IFN-γ: interferon-γ; KEGG: Kyoto Encyclopedia of Genes and Genomes; LPS: lipopolysaccharides; MF: molecular function.

accordingly ($t_{(8)} = 3.531$, $P = 0.0077 < 0.01$). Similar tendency was observed in collagen type (**Figure 7G** and **K**). The bladder function was measured with urodynamic test as the leaking point pressure decreased with BMDMs (LPS/IFN-γ + ES) so as to bladder compliance (leakage point pressure: $t_{(8)} = 4.790$, $P = 0.0014 < 0.01$; compliance: $t_{(8)} = 2.982$, $P = 0.0176 < 0.05$; **Figure 7H** and **I**). The volume of bladder was tested with high frequency microultrasoundgraphy was significantly different in crushed rats transplanted with BMDMs (LPS/IFN-γ) ($t_{(8)} = 8.186$, $P < 0.0001$). Meanwhile, it decreased in BMDMs (LPS/IFN-γ + ES) group ($t_{(8)} = 3.437$, $P = 0.0089 < 0.01$; **Figure 7J**). Generally, we found that crushed nerve without ES suffered from worse regeneration from the transplantation of LPS/IFN-γ-induced BMDMs. The BMDM polarisation induced by LPS/IFN-γ was reversed by ES , remodelling the microenvironment accordingly.

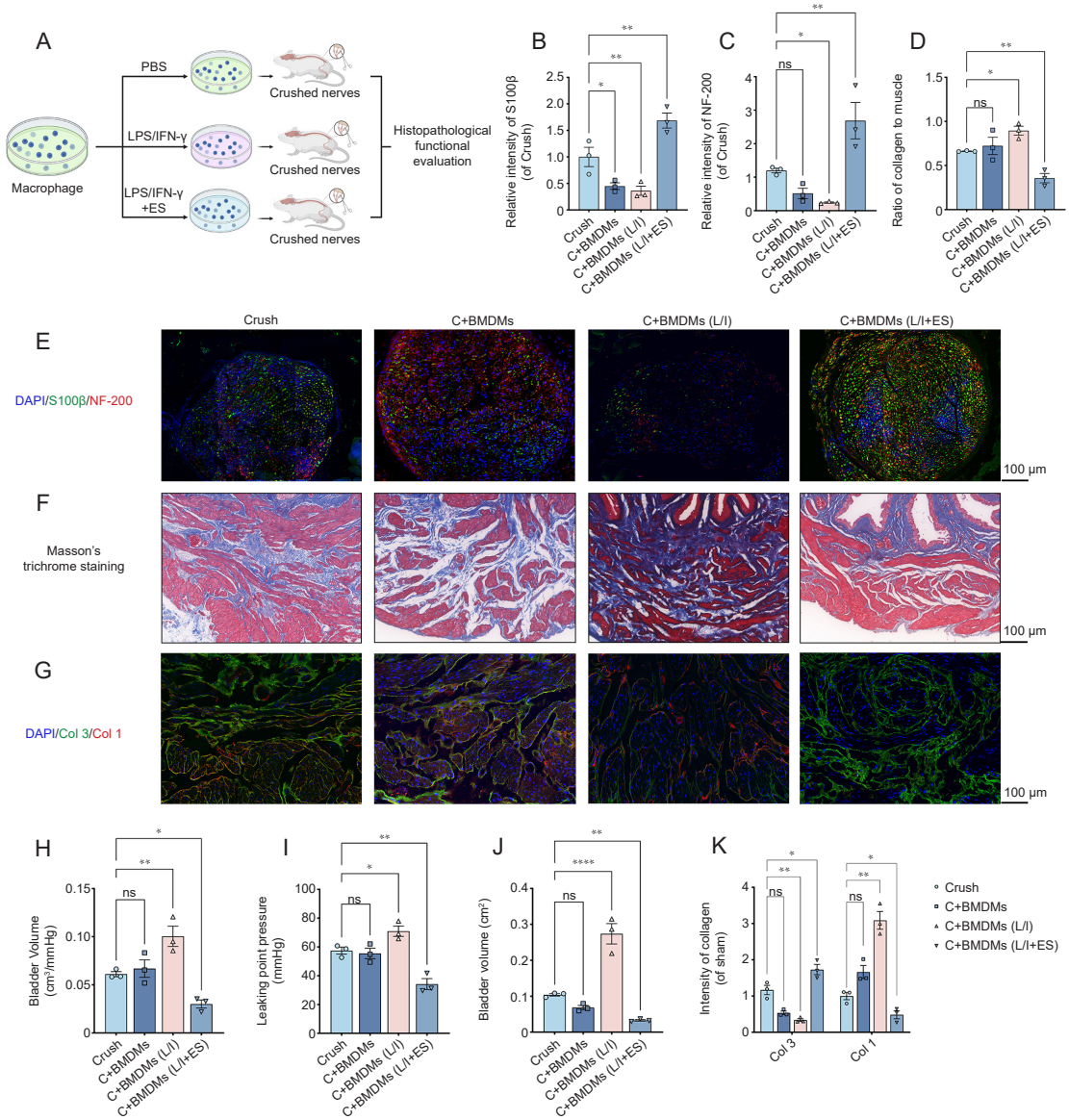

Figure 7. The replantation of BMDMs with LPS/IFN-γ induction and electrical stimulation. (A) The diagram of replantation of BMDMs with PBS, LPS/IFN-γ or LPS/IFN-γ + ES treatment into crushed sacral nerves. Created with BioRender.com. (B, C) The intensity of S100β (B) and neurofilament 200 (C) in immunofluorescence images of sacral nerves. (D) Ratio of collagen to muscle. The muscle was stained as red while collagen was stained as blue. (E) Representative images of S100β (green, Alexa Fluor 488) and neurofilament 200 (red, Alexa Fluor® 594) in crushed nerves. Scale bar: 100 μm. (F) Representative images of Masson's trichrome staining. Scale bar: 100 μm. (G) Representative images of Col 3 (green, Alexa Fluor 488) and Col 1 (red, Alexa Fluor® 594). Scale bar: 100 μm. (H, I) The bladder compliance (H) and leaking point pressure (I) with urodynamic test. (J) The bladder volume test in ultrasonography. (K) The intensity of Col 3 and Col 1 in immunofluorescence images. Data are shown as mean ± SEM (n = 3 per group). *P < 0.005, **P < 0.01, ****P < 0.0001 (one-way analysis of variance followed by Bonferroni's *post hoc* test). BMDM: bone marrow-derived macrophage; Col 1: collagen 1; Col 3: collagen 3; DAPI: 4′,6-diamidino-2-phenylindole; ES: electrical stimulation; IFN-γ: interferon-γ; LPS: lipopolysaccharides; ns: not significant; PBS: phosphate buffer saline.

Discussion

We developed a novel conductive membrane for *in vivo* sacral nerve ES by combining electrospinning of PCL/SF and in situ polymerisation of pyrrole. Obviously, we've seen many studies concerning the ES on injured nerves, most of which paid close attention to axon elongation or Schwann cells activation.[8, 75-77] Macrophage, however was less reported. This work demonstrated the important role of macrophage polarisation in peripheral nerve regeneration boosted by ES. Some researcher may argue that the traditional M1/M2 theory overcomplicated the vague and versatile macrophage spectrum therefore diminished the credibility of conclusion of experiments *in vitro*. In fact, our results from "back-transplantation" confirmed the direct ES on macrophage reversed the LPS/IFN-γ-induced pro-inflammation phenotype and, in the meantime, yielded an exclusive pro-regenerative effect when implanted back to crushed nerves. The idea came from a similar research[78] and was first applied in peripheral nerve-regeneration studies.

Moreover, our findings demonstrate that ES regulates macrophage activity during the initial phase of nerve regeneration, even when minimal macrophages are recruited to the site of injury, thereby attenuating inflammation. Previous study may insist on periodical stimulation[79-81] based on the theory that macrophage may fall easily into M1 without constant M2-related stimulation. According to our results, brief ES immediately after injury could alter immune microenvironment once for all to polarised recruited circulating macrophages. It is still unclear how it works and demands our further investigation.

Here, we found JAK-STAT signalling pathway and calcium signalling pathway involved in ES on macrophage through high-throughput sequencing analysis for the first time. We will carry out further analysis of the calcium channel blocker to show whether the voltage-gated calcium opening is the initial steps leading to polarisation shift. STAT family has seven members, expression of which can be distinguishedly regulated according to our results. In a word, macrophage response to same stimuli in varied extent due different STAT expression. However, the precise mechanisms by which calcium uptake influences the expression of STATs are currently under investigation.

The utilization of ES on the sacral nerve has gained significant attention due to promising clinical application of sacral nerve modulation in the treatment of neurogenic bladder, which has shown favourable rates of restoring bladder function. We took a step forward and found macrophage as a crucial regulator of sacral nerve regeneration. Next, Wang et al.[82] reported that the sacral spinal-vagal pathway may participate in the regulation of the GI disorder by sacral ES. The mechanisms of sacral nerve modulation have been clarified in similar studies conducted in other regions. By initiating stimulation at the onset of injury, we have provided evidence that early-stage ES facilitates sacral nerve regeneration after crush injury, thereby expanding the applicability of nerve modulation as a therapeutic modality.

Dielectric materials have long been investigated due to the susceptibility of nerves to mechanical damage, electric burns, and electrolytic effects. PPy possessed with excellent conductivity, was not suitable for biomaterial application for hardness. Most researcher take it as dopant in biocompatible material.[17, 83] In our study, we developed a membrane composed of PCL/SF with a PPy coating, which exhibited adequate biocompatibility and conductivity through *in situ* polymerization for *in vivo* ES, which was seldom used before. The method did not impair the excellent mechanical nature of electrospun PCL/SF fibre evidently for that the polymer was just coated onto surface fibre. Additionally, we used less pyrrole this way which attenuated possible remanent toxic monomer. We also over-dosed the oxidising agent compared to previous study[84] just in that case. However, we removed the membrane after 1 hour of ES, as its retention did not contribute to the regeneration of the crushed sacral nerve. This approach limited any potential damage.

In conclusion, the clinical management of sacral nerve injuries, which often involve complex damage, poses significant challenges. In our study, we employed ES as a therapeutic approach for sacral nerve crush injuries using a PPy-coated PCL/SF membrane. As we hypothesised, the ES improved neural regenerative potential and rescued the neurogenic bladder. Cell cytometry showed that macrophage polarisation shifted to M2 at 7th day post-injury in contrast to the enrichment of M1 in the damaged sacral nerve. Combining *in vitro* studies with transcriptome analysis, we have demonstrated that ES promotes the transition of macrophages from an M1 to an M2 phenotype by regulating the expression of Stat1/Stat3/Stat6. These findings highlight the distinctive contribution of macrophages to ES-induced nerve regeneration, unveiling a novel role in this process.

Author contributions

HC: Conceptualization, methodology, investigation and writing - original draft; JB: software, resources, data curation, writing - original draft and visualisation; XZ: validation, investigation, formal analysis and writing - original draft; NC: resources, investigation and data curation; QJ: methodology and formal analysis; ZR: visualisation and writing - review & editing; XL: validation and writing - review & editing; TS: formal analysis and visualisation; LL: methodology and software; WJ: supervision; YW: supervision, writing - review & editing and guarantor; JP: supervision and project administration; AS: supervision and funding acquisition. All authors approved the final version of the manuscript.

Financial support

This study was supported by Capital's Funds for Health Improvement and Research (No. CFH2022-2-5022).

Acknowledgement

We are grateful to Beijing PINS Medical Co., Ltd. for their support in providing the electrodes and pulse generator and technical data. And authors would like to thank all the reviewers who participated in the review and MJEditor (www.mjeditor.com) for its linguistic assistance during the preparation of this manuscript.

Conflicts of interest statement

The authors declare no conflict of the interest.

Additional file

Additional Figure 1: Verification of JAK/STAT signalling pathway and intracellular calcium.

1. Hamid, R.; Averbeck, M. A.; Chiang, H.; Garcia, A.; Al Mousa, R. T.; Oh, S. J.; Patel, A.; Plata, M.; Del Popolo, G. Epidemiology and pathophysiology of neurogenic bladder after spinal cord injury. *World J Urol.* **2018**, *36*, 1517-1527.
2. Li, J.; Li, S.; Wang, Y.; Shang, A. Functional, morphological and molecular characteristics in a novel rat model of spinal sacral nerve injury-surgical approach, pathological process and clinical relevance. *Sci Rep.* **2022**, *12*, 10026.
3. Gill, B. C.; Thomas, S.; Barden, L.; Jelovsek, J. E.; Meyer, I.; Chermansky, C.; Komesu, Y. M.; Menefee, S.; Myers, D.; Smith, A.; Mazloomdoost, D.; Amundsen, C. L. Intraoperative predictors of sacral neuromodulation implantation and treatment response: results from the ROSETTA trial. *J Urol.* **2023**, *210*, 331-340.
4. Liao, L. Evaluation and management of neurogenic bladder: what is new in China? *Int J Mol Sci.* **2015**, *16*, 18580-18600.
5. Gordon, T. Peripheral nerve regeneration and muscle reinnervation. *Int J Mol Sci.* **2020**, *21*, 8652.
6. Menorca, R. M.; Fussell, T. S.; Elfar, J. C. Nerve physiology:

mechanisms of injury and recovery. *Hand Clin.* **2013**, *29*, 317-330.
7. Dubový, P. Wallerian degeneration and peripheral nerve conditions for both axonal regeneration and neuropathic pain induction. *Ann Anat.* **2011**, *193*, 267-275.
8. Singh, B.; Xu, Q. G.; Franz, C. K.; Zhang, R.; Dalton, C.; Gordon, T.; Verge, V. M.; Midha, R.; Zochodne, D. W. Accelerated axon outgrowth, guidance, and target reinnervation across nerve transection gaps following a brief electrical stimulation paradigm. *J Neurosurg.* **2012**, *116*, 498-512.
9. Zigmond, R. E.; Echevarria, F. D. Macrophage biology in the peripheral nervous system after injury. *Prog Neurobiol.* **2019**, *173*, 102-121.
10. Zhou, D.; Huang, C.; Lin, Z.; Zhan, S.; Kong, L.; Fang, C.; Li, J. Macrophage polarization and function with emphasis on the evolving roles of coordinated regulation of cellular signaling pathways. *Cell Signal.* **2014**, *26*, 192-197.
11. Murray, P. J. Macrophage polarization. *Annu Rev Physiol.* **2017**, *79*, 541-566.
12. Liu, P.; Peng, J.; Han, G. H.; Ding, X.; Wei, S.; Gao, G.; Huang, K.; Chang, F.; Wang, Y. Role of macrophages in peripheral nerve injury and repair. *Neural Regen Res.* **2019**, *14*, 1335-1342.
13. Chen, P.; Piao, X.; Bonaldo, P. Role of macrophages in Wallerian degeneration and axonal regeneration after peripheral nerve injury. *Acta Neuropathol.* **2015**, *130*, 605-618.
14. Liu, P. S.; Wang, H.; Li, X.; Chao, T.; Teav, T.; Christen, S.; Di Conza, G.; Cheng, W. C.; Chou, C. H.; Vavakova, M.; Muret, C.; Debackere, K.; Mazzone, M.; Huang, H. D.; Fendt, S. M.; Ivanisevic, J.; Ho, P. C. α-ketoglutarate orchestrates macrophage activation through metabolic and epigenetic reprogramming. *Nat Immunol.* **2017**, *18*, 985-994.
15. Juckett, L.; Saffari, T. M.; Ormseth, B.; Senger, J. L.; Moore, A. M. The effect of electrical stimulation on nerve regeneration following peripheral nerve injury. *Biomolecules.* **2022**, *12*, 1856.
16. Chu, X. L.; Song, X. Z.; Li, Q.; Li, Y. R.; He, F.; Gu, X. S.; Ming, D. Basic mechanisms of peripheral nerve injury and treatment via electrical stimulation. *Neural Regen Res.* **2022**, *17*, 2185-2193.
17. Zhao, Y.; Liang, Y.; Ding, S.; Zhang, K.; Mao, H. Q.; Yang, Y. Application of conductive PPy/SF composite scaffold and electrical stimulation for neural tissue engineering. *Biomaterials.* **2020**, *255*, 120164.
18. Li, X.; Zhang, T.; Li, C.; Xu, W.; Guan, Y.; Li, X.; Cheng, H.; Chen, S.; Yang, B.; Liu, Y.; Ren, Z.; Song, X.; Jia, Z.; Wang, Y.; Tang, J. Electrical stimulation accelerates Wallerian degeneration and promotes nerve regeneration after sciatic nerve injury. *Glia.* **2023**, *71*, 758-774.
19. Keane, G. C.; Pan, D.; Roh, J.; Larson, E. L.; Schellhardt, L.; Hunter, D. A.; Snyder-Warwick, A. K.; Moore, A. M.; Mackinnon, S. E.; Wood, M. D. The effects of intraoperative electrical stimulation on regeneration and recovery after nerve isograft repair in a rat model. *Hand (N Y).* **2022**, *17*, 540-548.
20. Rouabhia, M.; Park, H.; Meng, S.; Derbali, H.; Zhang, Z. Electrical stimulation promotes wound healing by enhancing dermal fibroblast activity and promoting myofibroblast transdifferentiation. *PLoS One.* **2013**, *8*, e71660.
21. Rajendran, S. B.; Challen, K.; Wright, K. L.; Hardy, J. G. Electrical stimulation to enhance wound healing. *J Funct Biomater.* **2021**, *12*, 40.
22. Oliveira, K. M. C.; Barker, J. H.; Berezikov, E.; Pindur, L.; Kynigopoulos, S.; Eischen-Loges, M.; Han, Z.; Bhavsar, M. B.; Henrich, D.; Leppik, L. Electrical stimulation shifts healing/scarring towards regeneration in a rat limb amputation model. *Sci Rep.* **2019**, *9*, 11433.
23. Hu, L.; Klein, J. D.; Hassounah, F.; Cai, H.; Zhang, C.; Xu, P.; Wang, X. H. Low-frequency electrical stimulation attenuates muscle atrophy in CKD--a potential treatment strategy. *J Am Soc Nephrol.* **2015**, *26*, 626-635.
24. Schiavone, G.; Kang, X.; Fallegger, F.; Gandar, J.; Courtine, G.; Lacour, S. P. Guidelines to study and develop soft electrode systems for neural stimulation. *Neuron.* **2020**, *108*, 238-258.
25. Zhang, J.; Qiu, K.; Sun, B.; Fang, J.; Zhang, K.; Ei-Hamshary, H.; Al-Deyab, S. S.; Mo, X. The aligned core-sheath nanofibers with electrical conductivity for neural tissue engineering. *J Mater Chem B.* **2014**, *2*, 7945-7954.
26. Zheng, X. S.; Griffith, A. Y.; Chang, E.; Looker, M. J.; Fisher, L. E.; Clapsaddle, B.; Cui, X. T. Evaluation of a conducting elastomeric composite material for intramuscular electrode application. *Acta Biomater.* **2020**, *103*, 81-91.
27. Wu, S.; Qi, Y.; Shi, W.; Kuss, M.; Chen, S.; Duan, B. Electrospun conductive nanofiber yarns for accelerating mesenchymal stem cells differentiation and maturation into Schwann cell-like cells under a combination of electrical stimulation and chemical induction. *Acta Biomater.* **2022**, *139*, 91-104.
28. Wang, J.; Tian, L.; Chen, N.; Ramakrishna, S.; Mo, X. The cellular response of nerve cells on poly-l-lysine coated PLGA-MWCNTs aligned nanofibers under electrical stimulation. *Mater Sci Eng C Mater Biol Appl.* **2018**, *91*, 715-726.
29. Mao, W.; Lee, E.; Cho, W.; Kang, B. J.; Yoo, H. S. Cell-directed assembly of luminal nanofibril fillers in nerve conduits for peripheral nerve repair. *Biomaterials.* **2023**, *301*, 122209.
30. Guo, W.; Zhang, X.; Yu, X.; Wang, S.; Qiu, J.; Tang, W.; Li, L.; Liu, H.; Wang, Z. L. Self-powered electrical stimulation for enhancing neural differentiation of mesenchymal stem cells on graphene-poly(3,4-ethylenedioxythiophene) hybrid microfibers. *ACS Nano.* **2016**, *10*, 5086-5095.
31. Guan, Y.; Ren, Z.; Yang, B.; Xu, W.; Wu, W.; Li, X.; Zhang, T.; Li, D.; Chen, S.; Bai, J.; Song, X.; Jia, Z.; Xiong, X.; He, S.; Li, C.; Meng, F.; Wu, T.; Zhang, J.; Liu, X.; Meng, H.; Peng, J.; Wang, Y. Dual-bionic regenerative microenvironment for peripheral nerve repair. *Bioact Mater.* **2023**, *26*, 370-386.
32. Lee, J. Y.; Bashur, C. A.; Goldstein, A. S.; Schmidt, C. E. Polypyrrole-coated electrospun PLGA nanofibers for neural tissue applications. *Biomaterials.* **2009**, *30*, 4325-4335.
33. Sun, B.; Wu, T.; Wang, J.; Li, D.; Wang, J.; Gao, Q.; Bhutto, M. A.; El-Hamshary, H.; Al-Deyab, S. S.; Mo, X. Polypyrrole-coated poly(l-lactic acid-co-ε-caprolactone)/silk fibroin nanofibrous membranes promoting neural cell proliferation and differentiation with electrical stimulation. *J Mater Chem B.* **2016**, *4*, 6670-6679.
34. Hardy, J. G.; Cornelison, R. C.; Sukhavasi, R. C.; Saballos, R. J.; Vu, P.; Kaplan, D. L.; Schmidt, C. E. Electroactive tissue scaffolds with aligned pores as instructive platforms for biomimetic tissue engineering. *Bioengineering (Basel).* **2015**, *2*, 15-34.
35. Sapountzi, E.; Chateaux, J. F.; Lagarde, F. Combining electrospinning and vapor-phase polymerization for the production of polyacrylonitrile/ polypyrrole core-shell nanofibers and glucose biosensor application. *Front Chem.* **2020**, *8*, 678.
36. Wang, Y.; Yao, D.; Li, L.; Qian, Z.; He, W.; Ding, R.; Liu, H.; Fan, Y. Effect of electrospun silk fibroin-silk sericin films on macrophage polarization and vascularization. *ACS Biomater Sci Eng.* **2020**, *6*, 3502-3512.
37. National Research Council. *Guide for the Care and Use of Laboratory Animals, 8th edition.* National Academies Press: Washington, DC, USA.

2011.

38. Ayanwuyi, L.; Tokarska, N.; McLean, N. A.; Johnston, J. M.; Verge, V. M. K. Brief electrical nerve stimulation enhances intrinsic repair capacity of the focally demyelinated central nervous system. *Neural Regen Res.* **2022**, *17*, 1042-1050.
39. McLean, N. A.; Verge, V. M. Dynamic impact of brief electrical nerve stimulation on the neural immune axis-polarization of macrophages toward a pro-repair phenotype in demyelinated peripheral nerve. *Glia.* **2016**, *64*, 1546-1561.
40. Bailey, J. D.; Shaw, A.; McNeill, E.; Nicol, T.; Diotallevi, M.; Chuaiphichai, S.; Patel, J.; Hale, A.; Channon, K. M.; Crabtree, M. J. Isolation and culture of murine bone marrow-derived macrophages for nitric oxide and redox biology. *Nitric Oxide.* **2020**, *100-101*, 17-29.
41. Halimani, N.; Nesterchuk, M.; Andreichenko, I. N.; Tsitrina, A. A.; Elchaninov, A.; Lokhonina, A.; Fatkhudinov, T.; Dashenkova, N. O.; Brezgina, V.; Zatsepin, T. S.; Mikaelyan, A. S.; Kotelevtsev, Y. V. Phenotypic alteration of BMDM in vitro using small interfering RNA. *Cells.* **2022**, *11*, 2498.
42. Liu, Y.; Wu, Y.; Wang, C.; Hu, W.; Zou, S.; Ren, H.; Zuo, Y.; Qu, L. MiR-127-3p enhances macrophagic proliferation via disturbing fatty acid profiles and oxidative phosphorylation in atherosclerosis. *J Mol Cell Cardiol.* **2024**, *193*, 36-52.
43. Zhu, H. T.; Luo, J.; Peng, Y.; Cheng, X. F.; Wu, S. Z.; Zhao, Y. D.; Chang, L.; Sun, Z. J.; Dong, D. L. Nitazoxanide protects against experimental ulcerative colitis through improving intestinal barrier and inhibiting inflammation. *Chem Biol Interact.* **2024**, *395*, 111013.
44. Yoshida, M.; Kwon, A. T.; Qin, X. Y.; Nishimura, H.; Maeda, S.; Miyamoto, Y.; Yoshida, Y.; Hoshino, Y.; Suzuki, H. Transcriptome analysis of long non-coding RNAs in Mycobacterium avium complex-infected macrophages. *Front Immunol.* **2024**, *15*, 1374437.
45. Tian, L.; Zhao, J. L.; Kang, J. Q.; Guo, S. B.; Zhang, N.; Shang, L.; Zhang, Y. L.; Zhang, J.; Jiang, X.; Lin, Y. Astragaloside IV alleviates the experimental DSS-induced colitis by remodeling macrophage polarization through STAT signaling. *Front Immunol.* **2021**, *12*, 740565.
46. Cheung, W. A.; Johnson, A. F.; Rowell, W. J.; Farrow, E.; Hall, R.; Cohen, A. S. A.; Means, J. C.; Zion, T. N.; Portik, D. M.; Saunders, C. T.; Koseva, B.; Bi, C.; Truong, T. K.; Schwendinger-Schreck, C.; Yoo, B.; Johnston, J. J.; Gibson, M.; Evrony, G.; Rizzo, W. B.; Thiffault, I.; Younger, S. T.; Curran, T.; Wenger, A. M.; Grundberg, E.; Pastinen, T. Direct haplotype-resolved 5-base HiFi sequencing for genome-wide profiling of hypermethylation outliers in a rare disease cohort. *Nat Commun.* **2023**, *14*, 3090.
47. Carbon, S.; Ireland, A.; Mungall, C. J.; Shu, S.; Marshall, B.; Lewis, S. AmiGO: online access to ontology and annotation data. *Bioinformatics.* **2009**, *25*, 288-289.
48. Gene Ontology Consortium; Aleksander, S. A.; Balhoff, J.; Carbon, S.; Cherry, J. M.; Drabkin, H. J.; Ebert, D.; Feuermann, M.; Gaudet, P.; Harris, N. L.; Hill, D. P.; Lee, R.; Mi, H.; Moxon, S.; Mungall, C. J.; Muruganugan, A.; Mushayahama, T.; Sternberg, P. W.; Thomas, P. D.; Van Auken, K.; Ramsey, J.; Siegele, D. A.; Chisholm, R. L.; Fey, P.; Aspromonte, M. C.; Nugnes, M. V.; Quaglia, F.; Tosatto, S.; Giglio, M.; Nadendla, S.; Antonazzo, G.; Attrill, H.; Dos Santos, G.; Marygold, S.; Strelets, V.; Tabone, C. J.; Thurmond, J.; Zhou, P.; Ahmed, S. H.; Asanitthong, P.; Luna Buitrago, D.; Erdol, M. N.; Gage, M. C.; Ali Kadhum, M.; Li, K. Y. C.; Long, M.; Michalak, A.; Pesala, A.; Pritazahra, A.; Saverimuttu, S. C. C.; Su, R.; Thurlow, K. E.; Lovering, R. C.; Logie, C.; Oliferenko, S.; Blake, J.; Christie, K.; Corbani, L.; Dolan, M. E.; Drabkin, H. J.; Hill, D. P.; Ni, L.; Sitnikov, D.; Smith, C.; Cuzick, A.; Seager, J.; Cooper, L.; Elser, J.; Jaiswal, P.; Gupta, P.; Jaiswal, P.; Naithani, S.; Lera-Ramirez, M.; Rutherford, K.; Wood, V.; De Pons, J. L.; Dwinell, M. R.; Hayman, G. T.; Kaldunski, M. L.; Kwitek, A. E.; Laulederkind, S. J. F.; Tutaj, M. A.; Vedi, M.; Wang, S. J.; D'Eustachio, P.; Aimo, L.; Axelsen, K.; Bridge, A.; Hyka-Nouspikel, N.; Morgat, A.; Aleksander, S. A.; Cherry, J. M.; Engel, S. R.; Karra, K.; Miyasato, S. R.; Nash, R. S.; Skrzypek, M. S.; Weng, S.; Wong, E. D.; Bakker, E.; Berardini, T. Z.; Reiser, L.; Auchincloss, A.; Axelsen, K.; Argoud-Puy, G.; Blatter, M. C.; Boutet, E.; Breuza, L.; Bridge, A.; Casals-Casas, C.; Coudert, E.; Estreicher, A.; Livia Famiglietti, M.; Feuermann, M.; Gos, A.; Gruaz-Gumowski, N.; Hulo, C.; Hyka-Nouspikel, N.; Jungo, F.; Le Mercier, P.; Lieberherr, D.; Masson, P.; Morgat, A.; Pedruzzi, I.; Pourcel, L.; Poux, S.; Rivoire, C.; Sundaram, S.; Bateman, A.; Bowler-Barnett, E.; Bye, A. J. H.; Denny, P.; Ignatchenko, A.; Ishtiaq, R.; Lock, A.; Lussi, Y.; Magrane, M.; Martin, M. J.; Orchard, S.; Raposo, P.; Speretta, E.; Tyagi, N.; Warner, K.; Zaru, R.; Diehl, A. D.; Lee, R.; Chan, J.; Diamantakis, S.; Raciti, D.; Zarowiecki, M.; Fisher, M.; James-Zorn, C.; Ponferrada, V.; Zorn, A.; Ramachandran, S.; Ruzicka, L.; Westerfield, M. The Gene Ontology knowledgebase in 2023. *Genetics.* **2023**, *224*, iyad031.
49. Ashburner, M.; Ball, C. A.; Blake, J. A.; Botstein, D.; Butler, H.; Cherry, J. M.; Davis, A. P.; Dolinski, K.; Dwight, S. S.; Eppig, J. T.; Harris, M. A.; Hill, D. P.; Issel-Tarver, L.; Kasarskis, A.; Lewis, S.; Matese, J. C.; Richardson, J. E.; Ringwald, M.; Rubin, G. M.; Sherlock, G. Gene ontology: tool for the unification of biology. The Gene Ontology Consortium. *Nat Genet.* **2000**, *25*, 25-29.
50. Thomas, P. D.; Ebert, D.; Muruganujan, A.; Mushayahama, T.; Albou, L. P.; Mi, H. PANTHER: making genome-scale phylogenetics accessible to all. *Protein Sci.* **2022**, *31*, 8-22.
51. Szklarczyk, D.; Kirsch, R.; Koutrouli, M.; Nastou, K.; Mehryary, F.; Hachilif, R.; Gable, A. L.; Fang, T.; Doncheva, N. T.; Pyysalo, S.; Bork, P.; Jensen, L. J.; von Mering, C. The STRING database in 2023: protein-protein association networks and functional enrichment analyses for any sequenced genome of interest. *Nucleic Acids Res.* **2023**, *51*, D638-D646.
52. Maeng, W. Y.; Tseng, W. L.; Li, S.; Koo, J.; Hsueh, Y. Y. Electroceuticals for peripheral nerve regeneration. *Biofabrication.* **2022**, *14*, 042002.
53. Li, M.; Sun, X.; Zhao, J.; Xia, L.; Li, J.; Xu, M.; Wang, B.; Guo, H.; Yu, C.; Gao, Y.; Wu, H.; Kong, X.; Xia, Q. CCL5 deficiency promotes liver repair by improving inflammation resolution and liver regeneration through M2 macrophage polarization. *Cell Mol Immunol.* **2020**, *17*, 753-764.
54. Frangogiannis, N. G.; Ren, G.; Dewald, O.; Zymek, P.; Haudek, S.; Koerting, A.; Winkelmann, K.; Michael, L. H.; Lawler, J.; Entman, M. L. Critical role of endogenous thrombospondin-1 in preventing expansion of healing myocardial infarcts. *Circulation.* **2005**, *111*, 2935-2942.
55. Hegdekar, N.; Sarkar, C.; Bustos, S.; Ritzel, R. M.; Hanscom, M.; Ravishankar, P.; Philkana, D.; Wu, J.; Loane, D. J.; Lipinski, M. M. Inhibition of autophagy in microglia and macrophages exacerbates innate immune responses and worsens brain injury outcomes. *Autophagy.* **2023**, *19*, 2026-2044.
56. McArthur, S.; Juban, G.; Gobbetti, T.; Desgeorges, T.; Theret, M.; Gondin, J.; Toller-Kawahisa, J. E.; Reutelingsperger, C. P.; Chazaud, B.; Perretti, M.; Mounier, R. Annexin A1 drives macrophage skewing to accelerate muscle regeneration through AMPK activation. *J Clin Invest.* **2020**, *130*, 1156-1167.

57. Li, R.; Li, D.; Wu, C.; Ye, L.; Wu, Y.; Yuan, Y.; Yang, S.; Xie, L.; Mao, Y.; Jiang, T.; Li, Y.; Wang, J.; Zhang, H.; Li, X.; Xiao, J. Nerve growth factor activates autophagy in Schwann cells to enhance myelin debris clearance and to expedite nerve regeneration. *Theranostics.* **2020**, *10*, 1649-1677.
58. Nishi, K.; Izumi, H.; Tomonaga, T.; Nagano, C.; Morimoto, Y.; Horie, S. IL-6-mediated upregulated miRNAs in extracellular vesicles derived from lund human mesencephalic (LUHMES) cells: effects on astrocytes and microglia. *Biomolecules.* **2023**, *13*, 718.
59. Merchant, J. L.; Ding, L. Hedgehog signaling links chronic inflammation to gastric cancer precursor lesions. *Cell Mol Gastroenterol Hepatol.* **2017**, *3*, 201-210.
60. Xu, F.; Cui, W. Q.; Wei, Y.; Cui, J.; Qiu, J.; Hu, L. L.; Gong, W. Y.; Dong, J. C.; Liu, B. J. Astragaloside IV inhibits lung cancer progression and metastasis by modulating macrophage polarization through AMPK signaling. *J Exp Clin Cancer Res.* **2018**, *37*, 207.
61. Gaojian, T.; Dingfei, Q.; Linwei, L.; Xiaowei, W.; Zheng, Z.; Wei, L.; Tong, Z.; Benxiang, N.; Yanning, Q.; Wei, Z.; Jian, C. Parthenolide promotes the repair of spinal cord injury by modulating M1/M2 polarization via the NF-κB and STAT 1/3 signaling pathway. *Cell Death Discov.* **2020**, *6*, 97.
62. Zhang, X.; He, B.; Li, H.; Wang, Y.; Zhou, Y.; Wang, W.; Song, T.; Du, N.; Gu, X.; Luo, Y.; Wang, Y. SOCS3 attenuates GM-CSF/IFN-γ-mediated inflammation during spontaneous spinal cord regeneration. *Neurosci Bull.* **2020**, *36*, 778-792.
63. Zhao, S. J.; Kong, F. Q.; Jie, J.; Li, Q.; Liu, H.; Xu, A. D.; Yang, Y. Q.; Jiang, B.; Wang, D. D.; Zhou, Z. Q.; Tang, P. Y.; Chen, J.; Wang, Q.; Zhou, Z.; Chen, Q.; Yin, G. Y.; Zhang, H. W.; Fan, J. Macrophage MSR1 promotes BMSC osteogenic differentiation and M2-like polarization by activating PI3K/AKT/GSK3β/β-catenin pathway. *Theranostics.* **2020**, *10*, 17-35.
64. Hoare, J. I.; Rajnicek, A. M.; McCaig, C. D.; Barker, R. N.; Wilson, H. M. Electric fields are novel determinants of human macrophage functions. *J Leukoc Biol.* **2016**, *99*, 1141-1151.
65. Kurosawa, M.; Oda, M.; Domon, H.; Isono, T.; Nakamura, Y.; Saitoh, I.; Hayasaki, H.; Yamaguchi, M.; Kawabata, S.; Terao, Y. Streptococcus pyogenes CAMP factor promotes calcium ion uptake in RAW264.7 cells. *Microbiol Immunol.* **2018**, *62*, 617-623.
66. Thuraisingam, T.; Xu, Y. Z.; Eadie, K.; Heravi, M.; Guiot, M. C.; Greemberg, R.; Gaestel, M.; Radzioch, D. MAPKAPK-2 signaling is critical for cutaneous wound healing. *J Invest Dermatol.* **2010**, *130*, 278-286.
67. Takahashi, M.; Umehara, Y.; Yue, H.; Trujillo-Paez, J. V.; Peng, G.; Nguyen, H. L. T.; Ikutama, R.; Okumura, K.; Ogawa, H.; Ikeda, S.; Niyonsaba, F. The antimicrobial peptide human β-defensin-3 accelerates wound healing by promoting angiogenesis, cell migration, and proliferation through the FGFR/JAK2/STAT3 signaling pathway. *Front Immunol.* **2021**, *12*, 712781.
68. Xiao, X.; Xu, M.; Yu, H.; Wang, L.; Li, X.; Rak, J.; Wang, S.; Zhao, R. C. Mesenchymal stem cell-derived small extracellular vesicles mitigate oxidative stress-induced senescence in endothelial cells via regulation of miR-146a/Src. *Signal Transduct Target Ther.* **2021**, *6*, 354.
69. Zhang, X.; Rotllan, N.; Canfrán-Duque, A.; Sun, J.; Toczek, J.; Moshnikova, A.; Malik, S.; Price, N. L.; Araldi, E.; Zhong, W.; Sadeghi, M. M.; Andreev, O. A.; Bahal, R.; Reshetnyak, Y. K.; Suárez, Y.; Fernández-Hernando, C. Targeted suppression of miRNA-33 Using pHLIP improves atherosclerosis regression. *Circ Res.* **2022**, *131*, 77-90.
70. Creaney, J.; Patch, A. M.; Addala, V.; Sneddon, S. A.; Nones, K.; Dick, I. M.; Lee, Y. C. G.; Newell, F.; Rouse, E. J.; Naeini, M. M.; Kondrashova, O.; Lakis, V.; Nakas, A.; Waller, D.; Sharkey, A.; Mukhopadhyay, P.; Kazakoff, S. H.; Koufariotis, L. T.; Davidson, A. L.; Ramarao-Milne, P.; Holmes, O.; Xu, Q.; Leonard, C.; Wood, S.; Grimmond, S. M.; Bueno, R.; Fennell, D. A.; Pearson, J. V.; Robinson, B. W.; Waddell, N. Comprehensive genomic and tumour immune profiling reveals potential therapeutic targets in malignant pleural mesothelioma. *Genome Med.* **2022**, *14*, 58.
71. Sutherland, T. E.; Dyer, D. P.; Allen, J. E. The extracellular matrix and the immune system: A mutually dependent relationship. *Science.* **2023**, *379*, eabp8964.
72. Xu, X.; Gu, S.; Huang, X.; Ren, J.; Gu, Y.; Wei, C.; Lian, X.; Li, H.; Gao, Y.; Jin, R.; Gu, B.; Zan, T.; Wang, Z. The role of macrophages in the formation of hypertrophic scars and keloids. *Burns Trauma.* **2020**, *8*, tkaa006.
73. Zhang, Y.; Gao, Z.; Jiang, F.; Yan, H.; Yang, B.; He, Q.; Luo, P.; Xu, Z.; Yang, X. JAK-STAT signaling as an ARDS therapeutic target: status and future trends. *Biochem Pharmacol.* **2023**, *208*, 115382.
74. Wang, C.; Ma, C.; Gong, L.; Guo, Y.; Fu, K.; Zhang, Y.; Zhou, H.; Li, Y. Macrophage Polarization and Its Role in Liver Disease. *Front Immunol.* **2021**, *12*, 803037.
75. Bunn, S. J.; Lai, A.; Li, J. DC electric fields induce perpendicular alignment and enhanced migration in schwann cell cultures. *Ann Biomed Eng.* **2019**, *47*, 1584-1595.
76. Huang, J.; Ye, Z.; Hu, X.; Lu, L.; Luo, Z. Electrical stimulation induces calcium-dependent release of NGF from cultured Schwann cells. *Glia.* **2010**, *58*, 622-631.
77. Haastert-Talini, K.; Schmitte, R.; Korte, N.; Klode, D.; Ratzka, A.; Grothe, C. Electrical stimulation accelerates axonal and functional peripheral nerve regeneration across long gaps. *J Neurotrauma.* **2011**, *28*, 661-674.
78. Wang, N.; Wang, W.; Wang, X.; Mang, G.; Chen, J.; Yan, X.; Tong, Z.; Yang, Q.; Wang, M.; Chen, L.; Sun, P.; Yang, Y.; Cui, J.; Yang, M.; Zhang, Y.; Wang, D.; Wu, J.; Zhang, M.; Yu, B. Histone lactylation boosts reparative gene activation post-myocardial infarction. *Circ Res.* **2022**, *131*, 893-908.
79. Salm, D. C.; Horewicz, V. V.; Tanaka, F.; Ferreira, J. K.; de Oliveira, B. H.; Maio, J. M. B.; Donatello, N. N.; Ludtke, D. D.; Mazzardo-Martins, L.; Dutra, A. R.; Mack, J. M.; de, C. H. K. D.; Cargnin-Ferreira, E.; Salgado, A. S. I.; Bittencourt, E. B.; Bianco, G.; Piovezan, A. P.; Bobinski, F.; Moré, A. O. O.; Martins, D. F. Electrical stimulation of the auricular branch vagus nerve using random and alternating frequencies triggers a rapid onset and pronounced antihyperalgesia via peripheral annexin A1-formyl peptide receptor 2/ALX pathway in a mouse model of persistent inflammatory pain. *Mol Neurobiol.* **2023**, *60*, 2889-2909.
80. Wu, H.; Dong, H.; Tang, Z.; Chen, Y.; Liu, Y.; Wang, M.; Wei, X.; Wang, N.; Bao, S.; Yu, D.; Wu, Z.; Yang, Z.; Li, X.; Guo, Z.; Shi, L. Electrical stimulation of piezoelectric BaTiO3 coated Ti6Al4V scaffolds promotes anti-inflammatory polarization of macrophages and bone repair via MAPK/JNK inhibition and OXPHOS activation. *Biomaterials.* **2023**, *293*, 121990.
81. Wang, J. Y.; Yuan, Y.; Zhang, S. Y.; Lu, S. Y.; Han, G. J.; Bian, M. X.; Huang, L.; Meng, D. H.; Su, D. H.; Xiao, L.; Xiao, Y.; Zhang, J.; Gong, N. J.; Jiang, L. B. Remodeling of the intra-conduit inflammatory microenvironment to improve peripheral nerve regeneration with a neuromechanical matching protein-based conduit. *Adv Sci (Weinh).* **2024**, *11*, e2302988.
82. Wang, X.; Zhang, S.; Pasricha, P. J.; Chen, J. D. Z. Ameliorating effects

of sacral neuromodulation on gastric and small intestinal dysmotility mediated via a sacral afferent-vagal efferent pathway. *Neurogastroenterol Motil.* **2020**, *32*, e13837.

83. Huang, J.; Hu, X.; Lu, L.; Ye, Z.; Zhang, Q.; Luo, Z. Electrical regulation of Schwann cells using conductive polypyrrole/chitosan polymers. *J Biomed Mater Res A.* **2010**, *93*, 164-174.

84. Tsui, J. H.; Ostrovsky-Snider, N. A.; Yama, D. M. P.; Donohue, J. D.; Choi, J. S.; Chavanachat, R.; Larson, J. D.; Murphy, A. R.; Kim, D. H. Conductive silk-polypyrrole composite scaffolds with bioinspired nanotopographic cues for cardiac tissue engineering. *J Mater Chem B.* **2018**, *6*, 7185-7196.

Received: March 27, 2024
Revised: May 18, 2024
Accepted: June 22, 2024
Available online: June 28, 2024